JOURNAL OF COMPUTATIONAL PHYSICS 105, 233–251 (1993)

Boundary Conditions for Open Boundaries for the Incompressible Navier–Stokes Equation

B. CHRISTER V. JOHANSSON

The Royal Institute of Technology, NADA - C2M2, S-100 44 Stockholm, Sweden

Received March 4, 1991; revised August 3, 1992

In this paper we investigate new boundary conditions for the incompressible, time-dependent Navier–Stokes equation. Especially inflow and outflow conditions are considered. The equations are linearized around a constant flow, so that we can use Laplace–Fourier technique to investigate the strength of boundary layers at open boundaries. Such layers are unphysical, and new boundary conditions are proposed so that these boundary layers are suppressed. We also show that the boundary conditions we propose do not produce divergence. Furthermore, they give solutions that do not grow in time, as long as the forcing function in the system does not. We also discuss the numerical treatment of boundaries when fourth-order accurate finite difference operators are used to approximate spatial derivatives. Using higher order methods introduces eigensolutions with boundary layer thickness of the same order of magnitude as the grid size. These eigensolutions have to be suppressed in order to not destroy the fourth-order accuracy of the method. Numerical results for the non-linear Navier–Stokes equation, together with the new boundary conditions, are presented. These calculations confirm that the results for the linearized problem hold for the non-linear problem as well.

1. INTRODUCTION

In this paper we investigate boundary conditions for the Navier–Stokes equation for incompressible fluid flow. In numerical calculations one often makes the calculation domain smaller than the physical domain in consideration by introducing open boundaries, i.e., inflow and outflow. For physical boundaries, such as solid wall and free surface, one can use physical arguments to derive boundary conditions. As open boundaries do not exist in reality, there is no direct physical argument for deriving boundary conditions for such boundaries.

It is well known that the solution of the Navier–Stokes equation can contain boundary layers. This is a true physical phenomenon when the boundary in consideration is, for instance, a solid wall. However, we will in this paper see that the solution can also contain boundary layers at open boundaries. Such layers are unphysical. However, when using numerical methods we must resolve them by making grid refinements near the boundaries, the boundary layers will otherwise cause wiggles. We should therefore define our boundary conditions in such a way that the boundary layers do not occur at all at open boundaries. The use of this criterion to construct boundary conditions for open boundaries was introduced in [2]. The general way to suppress the boundary layers is to let a normal derivative of a high order of some independent variables be zero at the boundary.

In this paper we construct new boundary conditions for inflow and outflow. These conditions suppress boundary layers effectively.

We model an inflow or outflow boundary by linearizing the incompressible Navier–Stokes equation around a constant flow. The so derived equation is solved analytically by Laplace–Fourier technique. For small viscosity the fundamental solution is shown to contain very different length scales. We identify the boundary layer part of the solution as the eigensolution to which the shortest length scale belong. We propose new, previously unknown, boundary conditions such that

(i) the boundary layer part of the fundamental solution is effectively suppressed.

Two more requirements on the boundary conditions are imposed, namely, they must be chosen so that

(ii) the solution does not grow in time, if the forcing function does not, and

(iii) no divergence that can spread far into the domain is produced at the boundary.

Letting u be the velocity component normal and v the component tangential to the boundary $x = 0$, we suggest the inflow boundary conditions

$$\begin{pmatrix} u \\ \dfrac{\partial^r v}{\partial x^r} \\ u_x + v_y \end{pmatrix}(0, y, t) = \begin{pmatrix} u_0 \\ v_0^r \\ 0 \end{pmatrix}(y, t), \qquad r = 0 \text{ or } 1 \text{ or } 2, \qquad (1)$$

where u_0 and v_0^r are given inflow profiles. These conditions

0021-9991/93 $5.00

fulfill the three requirements above. For the choice $v_0^r = 0$, the inflow boundary layer will be weaker, the larger r we use. However, *if $r \geqslant 3$ the solution will grow in time, even if* the forcing function does not. We recommend using $r = 2$.

If the last condition is not properly fulfilled, so that $u_x + v_y = \delta_0(y, t) \neq 0$ at $x = 0$, the divergence δ_0 will be convected far into the domain. We also point out that the boundary condition for the solid wall and the slip condition are special cases of the inflow condition (1).

We suggest the outflow boundary conditions

$$\begin{pmatrix} \dfrac{\partial^j u}{\partial x^j} \\ \dfrac{\partial^q v}{\partial x^q} \\ p \end{pmatrix} (0, y, t) = \begin{pmatrix} 0 \\ 0 \\ p_0 \end{pmatrix} (y, t). \tag{2}$$

These conditions fulfill the three requirements above as well. The higher values of j and q we use, the weaker the outflow boundary layer will be.

The choice $j = q + 1$ will give a solution that is divergence-free. However, if $j \neq q + 1$ and if the viscosity v is small, the divergence will be confined to the outflow boundary layer. This layer will be weak if we choose j and q large. Hence, in this case the requirement $j = q + 1$ is not very important, as long as j and q are large enough. Compare this to the inflow case where it is very important to have the condition $u_x + v_y = 0$ fulfilled at the boundary. We recommend using $j = 3$ and $q = 2$. In case the viscosity is small, we can also use $j = 2$ and $q = 2$.

The generalization of the boundary conditions above to three dimensions is straightforward. At each boundary we will need one more condition, and this is formed by treating the third velocity component in the same way as we treat v.

The concept of well-posedness is very important in numerical analysis for partial differential equations [2–6]. Well-posedness means that small disturbances cannot grow arbitrarily fast in time. As numerical methods always introduce small disturbances, we cannot solve ill-posed problems with numerical methods if no extra smoothing conditions are imposed to the problem. In [2–4] it is shown that the boundary conditions (1) and (2) are such that the problem derived by linearization around in arbitrary, smooth flow is well-posed in the generalized sense.

The rest of this paper is arranged as follows. In Section 2 we define the model problem for open boundaries. In Section 3 we discuss the solution of this problem via taking the Laplace transform in time and the Fourier transform in space. We derive the fundamental solution on the Laplace–Fourier transform side. The inverse transform is discussed and we give a theorem saying that if the solution on the Laplace–Fourier transform side has a pole at $s = s_p$, then the solution on the time-space side will grow in time as $e^{\text{Real}(s_p)t}$. This is of great importance, as the boundary condition can introduce such poles.

In Section 4 we discuss boundary layers. It is shown that the fundamental solution can have two very different length scales, and we identify the boundary layer part as the eigen-solution to which the shortest length scale belongs. In terms of the arbitrary constants in the fundamental solution we give criteria for when the boundary layers are weak. We also show how boundary layers on the Laplace–Fourier transform side correspond to boundary layers on the time-space side.

In Section 5 we apply the boundary conditions (1) and (2) to the fundamental solution and determine the integration constants. We show that prescribing a derivative of high order will suppress the boundary layers efficiently. We also discuss the divergence and the growth rate of the solution.

In Section 6 we present fourth-order accurate numerical solutions of the time-dependent, non-linear Navier–Stokes equation in a two-dimensional straight channel. The boundary layers predicted by the linear model problem is shown to occur in the solution of the non-linear problem as well. Furthermore, giving derivatives of high order as boundary condition give rise to weak boundary layers also in the non-linear case.

In Section 6 we also discuss the use of fourth-order accurate finite difference methods for the numerical solution of initial-boundary value problems. The use of fourth-order finite difference approximations of spatial derivatives introduces numerical boundary layers with the same thickness as the grid size. In order to obtain the fourth-order accuracy, these numerical boundary layers has to be suppressed. The high order method will also require extra numerical boundary conditions in order to be well defined. By a simple model problem we show a technique to define the extra boundary condition in such a way that the numerical boundary layers are suppressed. We use this technique to define the extra boundary conditions for the fourth-order approximation of the non-linear Navier–Stokes equation.

2. A MODEL PROBLEM FOR OPEN BOUNDARIES: THE LINEARIZATION AROUND A CONSTANT FLOW

The pressure formulation of the incompressible Navier–Stokes equation is

$$u'_t + u'u'_x + v'v'_y - vu'_{xx} - vu'_{yy} + p'_x = 0 \tag{3.a}$$

$$v'_t + u'v'_x + v'v'_y - vv'_{xx} - vv'_{yy} + p'_y = 0 \tag{3.b}$$

$$p'_{xx} + p'_{yy} + u'^2_x + 2v'_x u'_y + v'^2_y = 0. \tag{3.c}$$

Here the restriction to two space dimensions is no real restriction, as we could treat the z-direction in the same way

as we will treat the y-direction. The last equation is derived by taking the x-derivative of the first equation, adding the y-derivative of the second and using the incompressibility condition $u'_x + v'_y = 0$.

Linearizing (3) around a constant flow in the domain $0 \leqslant x < \infty$, $0 \leqslant y \leqslant 2\pi$, $0 \leqslant t < \infty$, yields

$$u_t + Uu_x + Vu_y - \nu u_{yy} - \nu u_{xx} + p_x = 0, \quad 0 \leqslant x < \infty, \quad 0 \leqslant y \leqslant 2\pi, \quad 0 \leqslant t < \infty, \tag{4.a}$$

$$v_t + Uv_x + Vv_y - \nu v_{yy} - \nu v_{xx} + p_y = 0, \quad 0 \leqslant x < \infty, \quad 0 \leqslant y \leqslant 2\pi, \quad 0 \leqslant t < \infty, \tag{4.b}$$

$$p_{xx} + p_{yy} = 0, \quad 0 \leqslant x < \infty, \quad 0 \leqslant y \leqslant 2\pi, \quad 0 \leqslant t < \infty. \tag{4.c}$$

We apply boundary conditions at $x = 0$ and require the solution to be 2π-periodic in the y-direction. The boundary condition at $x = 0$ will be written as

$$B(\partial/\partial x, \partial/\partial y, \partial/\partial t)\begin{pmatrix} u \\ v \\ p \end{pmatrix} = g(y, t), \quad x = 0, \quad 0 \leqslant y \leqslant 2\pi, \quad 0 \leqslant t < \infty. \tag{4.d}$$

B is a differential operator with constant coefficients. B can be, for instance, 1 (Dirichlet condition) or $\partial/\partial x$ (Neumann condition). We consider a simple class of forcing functions g and for simplicity demand that all the derivatives $\partial^{q_2+q_3} g/\partial y^{q_2}\,\partial t^{q_3}$ exist and that g and all its derivatives vanish identically at $t = 0$ and for $t \geqslant T_0(g)$. Furthermore, we demand that

$$\int_0^{2\pi} g(y, t)\, dy = 0, \qquad t \geqslant 0.$$

The solution must vanish at $x = \infty$, and as a side condition we demand

$$\int_0^\infty e^{-2\eta t}(\|u(\cdot, \cdot, t)\|^2 + \|v(\cdot, \cdot, t)\|^2 + \|p(\cdot, \cdot, t)\|^2)\, dt < \infty, \qquad \eta > \eta_0, \tag{4.e}$$

for some $\eta_0 \in R$. Here $\|h(\cdot, \cdot, t)\|$ is the L_2-norm of h, that is, $\|h(\cdot, \cdot, t)\|^2 = \int_0^\infty \int_0^{2\pi} h^2\, dy\, dx$.

Equation (4.e) can be considered as a boundary condition at $x = \infty$. The reason that we use the condition (4.e) and not, for instance, $\begin{pmatrix} u \\ v \\ p \end{pmatrix} \to 0$ as $x \to \infty$, is that if we use (4.e) as the side condition we can use Parseval's relation to derive a side condition for the Laplace–Fourier transform of $\begin{pmatrix} u \\ v \\ p \end{pmatrix}$. We let $\begin{pmatrix} u \\ v \\ p \end{pmatrix}$ vanish at $t = 0$, i.e.,

$$\begin{pmatrix} u \\ v \\ p \end{pmatrix}(x, y, 0) = 0, \qquad 0 \leqslant x < \infty, \quad 0 \leqslant y \leqslant 2\pi. \tag{4.f}$$

The half space problem (4) contains one boundary, namely $x = 0$. If $U > 0$ the boundary $x = 0$ is an inflow boundary, if $U < 0$ the boundary $x = 0$ is an outflow boundary, and if $U = 0$ the boundary $x = 0$ is a boundary through which no fluid passes. Hence, by choosing $U > 0$, $U < 0$, and $U = 0$ we will use the model problem (4) to investigate boundary conditions for inflow, outflow, and solid wall.

3. SOLUTION VIA THE LAPLACE–FOURIER TRANSFORM

3.1. The Fundamental Solution

We start with defining some notations. For a function $h = h(x, y, t)$, for $\mathrm{Real}(s) = \eta \geqslant \eta_0$ and for $\omega \in Z$, define

$$\hat{h}(x, \omega, s) = \frac{1}{2\pi}\int_0^{2\pi}\int_0^\infty e^{-st}e^{-i\omega y}h(x, y, t)\, dt\, dy$$

(the Laplace–Fourier transform)

and

$$h(x, y, t) = \frac{1}{2\pi i}\int_{\eta - i\infty}^{\eta + i\infty} \sum_{\omega = -\infty}^{\infty} e^{st}e^{i\omega y}\hat{h}(x, \omega, s)\, ds$$

(the inverse Laplace–Fourier transform).

Taking the Laplace–Fourier transform of the problem (4) yields

$$s\hat{u} + U\hat{u}_x + i\omega V\hat{u} - \nu\hat{u}_{xx} + \nu\omega^2\hat{u} + \hat{p}_x = 0, \quad 0 \leqslant x < \infty, \quad \omega \in Z, \tag{5.a}$$

$$s\hat{v} + U\hat{v}_x + i\omega V\hat{v} - \nu\hat{v}_{xx} + \nu\omega^2\hat{v} + i\omega\hat{p} = 0, \quad 0 \leqslant x < \infty, \quad \omega \in Z, \tag{5.b}$$

$$\hat{p}_{xx} - \omega^2\hat{p} = 0, \qquad 0 \leqslant x < \infty, \quad \omega \in Z, \tag{5.c}$$

$$B(\partial/\partial x, i\omega, s)\begin{pmatrix} \hat{u} \\ \hat{v} \\ \hat{p} \end{pmatrix} = \hat{g}(\omega, s), \qquad x = 0, \quad \omega \in Z, \tag{5.d}$$

$$\int_{-\infty}^\infty (\|\hat{u}(\cdot, \cdot, \eta + i\xi)\|^2 + \|\hat{v}(\cdot, \cdot, \eta + i\xi)\|^2 + \|\hat{p}(\cdot, \cdot, \eta + i\xi)\|^2)\, d\xi < 0, \qquad \eta > \eta_0. \tag{5.e}$$

From the definition of the Laplace–Fourier transform and the properties of g we obtain

$$|\omega^{q_2} s^{q_3} \hat{g}(\omega, s)| \leqslant \max_{\substack{0 \leqslant y \leqslant 2\pi \\ 0 \leqslant t \leqslant T_0}} \left| \frac{\partial^{q_2+q_3} g(y,t)}{\partial y^{q_2}\, \partial t^{q_3}} \right| \cdot \frac{1 - e^{-\mathrm{Real}(s) T_0}}{\mathrm{Real}(s)}$$
$$= K(g, q_1, q_2) \cdot \frac{1 - e^{-\mathrm{Real}(s) T_0}}{\mathrm{Real}(s)}, \qquad (5.f)$$

that is, the Laplace–Fourier transform of g decays fast as $|\omega| \to \infty$ or $|s| \to \infty$, $\mathrm{Real}(s) \geqslant \eta_0$, any $\eta_0 \in R$. Note that $\hat{g}(0, s) = 0$, which for the boundary conditions we will consider will lead to $\begin{pmatrix} \hat{u} \\ \hat{v} \\ \hat{p} \end{pmatrix}(x, 0, s) = 0$. From here on we therefore only consider $\omega \in Z \setminus \{0\}$.

The fundamental solution of (5.a)–(5.c), together with the side condition (5.e), is

$$\begin{pmatrix} \hat{u} \\ \hat{v} \\ \hat{p} \end{pmatrix} = \alpha_1 \cdot \begin{pmatrix} \dfrac{|\omega|}{\omega} \\ -i \\ -\dfrac{-s + U \cdot |\omega| - i\omega V}{\omega} \end{pmatrix} \cdot e^{-|\omega| x}$$
$$+ \alpha_u \cdot \begin{pmatrix} 1 \\ 0 \\ 0 \end{pmatrix} \cdot e^{-\kappa_2 x} + \alpha_v \cdot \begin{pmatrix} 0 \\ 1 \\ 0 \end{pmatrix} \cdot e^{-\kappa_2 x}, \qquad (6)$$

for $\mathrm{Real}(s) > -\nu\omega^2$ and $s \neq U|\omega| - i\omega V$, and

$$\begin{pmatrix} \hat{u} \\ \hat{v} \\ \hat{p} \end{pmatrix} = \begin{pmatrix} \alpha_u \\ \alpha_v \\ \alpha_p \end{pmatrix} \cdot e^{-|\omega| x} + \alpha_p \cdot x \cdot \begin{pmatrix} \dfrac{|\omega|}{2\nu|\omega| + U} \\ \dfrac{-i\omega}{2\nu|\omega| + U} \\ 0 \end{pmatrix} \cdot e^{-|\omega| x}, \qquad (7)$$

for $\mathrm{Real}(s) > -\nu\omega^2$ and $s = U|\omega| - i\omega V$. Here

$$\kappa_1 = |\omega| \qquad (8.a)$$
$$\kappa_2 = -\frac{U}{2\nu} + \left(\frac{U^2}{4\nu^2} + \omega^2 + \frac{s + i\omega V}{\nu} \right)^{1/2}. \qquad (8.b)$$

With the root we mean the branch with positive real part, i.e., $\mathrm{Real}(z^{1/2}) \geqslant 0$, and hence $\mathrm{Real}(\kappa_2) > 0$. α_1, α_u, and α_v in (6) and α_u, α_v, and α_p in (7) are arbitrary constants that will be determined by the boundary condition (5.d).

Before we specify and apply the boundary condition (5.d), we will in Section 3.2 and Section 4 discuss the solution on the time-space side. We will in general terms discuss the growth rate in time and the boundary layers.

3.2. The Inverse Laplace–Fourier Transform and the Growth Rate in Time

If the solution $\begin{pmatrix} \hat{u} \\ \hat{v} \\ \hat{p} \end{pmatrix}$ is analytic for $\mathrm{Real}(s) \geqslant \eta_0$ and if for all integers $q_1 \geqslant 0$, $q_2 \geqslant 0$, and $q_3 \geqslant 0$ and for all s with $\mathrm{Real}(s) \geqslant \eta_0$ we have

$$\left| \omega^{q_2} s^{q_3} \frac{\partial^{q_1}}{\partial x^{q_1}} \begin{pmatrix} \hat{u} \\ \hat{v} \\ \hat{p} \end{pmatrix}(x, \omega, s) \right| \leqslant K(q_1, q_2, q_3, \eta_0),$$

where K is independent of ω and s, then all the x-, y-, and t-derivatives of the inverse Laplace–Fourier transform exist and can be found by taking these derivatives inside the integral and the sum in the inverse transform formula. Furthermore, by the inverse Laplace–Fourier transform formula we easily obtain

$$\left| \begin{pmatrix} u \\ v \\ p \end{pmatrix}(x, y, t) \right| \leqslant K \cdot e^{\eta_0 t}.$$

However, we will see in the next lemma that if the solution on the Laplace transform side has a pole of order one at $s = s_p$, then the solution on the time side will grow as $e^{\mathrm{Real}(s_p) t}$. This means that if the boundary condition (5.d) allows solutions with a pole with $\mathrm{Real}(s_p) > 0$, then the solution on the time side will grow exponentially in time.

LEMMA 3.1. *Let $\tilde{h}$ be the Laplace transform of h. Let $\tilde{h} = \tilde{h}(s)$ be analytic for* $\mathrm{Real}(s) \geqslant \eta_0$. *Let*

$$(1 + |s|) \cdot |\tilde{h}(s)| \leqslant K, \qquad \mathrm{Real}(s) \geqslant \eta_0$$

for some K. Let $\mathrm{Real}(s_p) = \eta_p > \eta_0$. *Then, for any integer $q \geqslant 1$, the inverse Laplace transform of $\tilde{h}(s)/(s - s_p)$ is*

$$\tilde{h}(s_p) \cdot e^{s_p t} \cdot (1 + O(t^{-q})).$$

Outline of the Proof. Calculating the inverse Laplace transform along the line $\mathrm{Real}(s) = \eta_p + t^{-1}$ and using residue calculus proves the lemma. For more details, see [2]. ∎

4. LENGTH SCALES AND THE EXISTENCE OF BOUNDARY LAYERS

4.1. General Discussion

We will now see how a boundary layer in the Laplace–Fourier transform of a function corresponds to a boundary layer in the function itself. Let $h = h(x, y, t)$. There are

several ways to define the boundary layer thickness θ. One is to use a weighted L_2-norm and define

$$\theta_\eta = \frac{\int_0^\infty e^{-2\eta t} \|h(\cdot, \cdot, t)\|^2 \, dt}{\int_0^\infty e^{-2\eta t} \|h(0, \cdot, t)\|^2 \, dt}.$$

This definition of the boundary layer thickness was first introduced in [2] and is very useful when using the Laplace–Fourier transform. Indeed, by (6) we see that the fundamental solution of the problem (5) takes the form

$$\tilde{h}(x, \omega, s) = \alpha(\omega, s) \cdot e^{-\kappa(\omega, s) \cdot x}, \qquad \text{Real}(\kappa) > 0,$$

where $\text{Real}(\kappa)$ increases as $|\omega|$, $|\text{Im}(s)|$ or $\text{Real}(s) \geqslant 0$ increases. By Parseval's relation we obtain

$$\theta_\eta = \frac{\int_{-\infty}^{\infty} \sum_{\omega=-\infty}^{\infty} |\alpha(\omega, s)|^2 / (2\text{Real}(\kappa(\omega, s))) \, d\xi}{\int_{-\infty}^{\infty} \sum_{\omega=-\infty}^{\infty} |\alpha(\omega, s)|^2 \, d\xi}, \qquad s = \eta + i\xi, \quad \eta \geqslant \eta_0. \tag{9}$$

Therefore, if $\text{Real}(\kappa)$ is large for all values of ω and ξ for which α is large, then the boundary layer thickness is small. On the other hand, if $\text{Real}(\kappa)$ is small, then the boundary layer thickness is large.

4.2. Boundary Layers in the Fundamental Solution

The expression (9), together with the fundamental solution (6), can be used to investigate how to avoid boundary layers in the solution of (4). Equation (6) shows the existence of two length scales in the x-direction, namely $1/|\omega|$ and $1/\text{Real}(\kappa_2)$. The root κ_2, corresponding to the length scale $1/\text{Real}(\kappa_2)$, can obtain very different values, and we will now discuss this.

Inflow

In order to study inflow we consider the case $U > 0$ and for simplicity let $V = 0$. By (5.f) the forcing function $\hat{g}$ decays very fast for large ω and s. If this holds true also for the coefficients α_1, α_u, and α_v, the solution on the time-space side will essentially be determined by the expression (6) for small $|\omega|$ and $|s|$. It is therefore of interest to consider the case

$$\nu \ll \frac{U}{|\omega|}, \qquad \nu \ll \frac{U^2}{|s|}.$$

From (8.b) we obtain

$$\text{Real}(\kappa_2) = \text{Real}\left(-\frac{U}{2\nu} + \frac{U}{2\nu}\left(1 + \frac{4\nu^2\omega^2}{U^2} + \frac{4\nu s}{U^2}\right)^{1/2}\right) = \frac{\eta}{U} + \frac{\nu\omega^2}{U} + \frac{\nu(\xi^2 - \eta^2)}{U^3} + O(\nu^2),$$

where $s = \eta + i\xi$. If $g(y, t)$ contains rather high frequencies in y (for instance, a step which is slightly smoothed out), but varies slowly in time, $\hat{g}$ will decay faster with increasing $|s|$ than with increasing $|\omega|$. It is therefore relevant to consider $|s|/U \ll |\omega|$. This yields

$$\text{Real}(\kappa_2) \approx \frac{\eta}{U} + \frac{\nu\omega^2}{U} + \frac{\nu(\xi^2 - \eta^2)}{U^3} \ll \frac{\eta}{U} + |\omega| + \frac{|\xi|}{U} \approx |\omega|.$$

Hence, $\text{Real}(\kappa_2) \ll |\omega|$. Therefore,

$$\alpha_1 \cdot \begin{pmatrix} \dfrac{|\omega|}{\omega} \\ -i \\ -\dfrac{-s + U \cdot |\omega| - i\omega V}{\omega} \end{pmatrix} \cdot e^{-|\omega| x}$$

can be interpreted as the boundary layer part of the fundamental solution (6). If we could make $\alpha_1 = 0$, the boundary layer would be completely eliminated. In Section 5 we will propose boundary conditions such that α_1 becomes small compared to α_u and α_v. This means that we make the boundary layers weak. Hence, we have:

> *Inflow criterion for weak boundary layers.* The inflow boundary layers in the fundamental solution (6) are weak if α_1 is small compared to α_u and α_v.

Outflow

In order to study outflow we consider the case $U < 0$. From (8.b) we derive

$$\text{Real}(\kappa_2) > \max\left\{ \frac{|U|}{\nu}, \frac{|U|}{2\nu} + |\omega| \right\}.$$

As in the inflow case we consider

$$\nu \ll |U|/|\omega|$$

and we obtain $\text{Real}(\kappa_2) > |U|/\nu \gg |\omega|$. Hence, in the outflow case it is

$$\alpha_u \cdot \begin{pmatrix} 1 \\ 0 \\ 0 \end{pmatrix} \cdot e^{-\kappa_2 x} + \alpha_v \cdot \begin{pmatrix} 0 \\ 1 \\ 0 \end{pmatrix} \cdot e^{-\kappa_2 x}$$

that can be interpreted as the boundary layer part of the fundamental solution (6). In Section 5 we will give

boundary conditions that make α_u and α_v small compared to α_1, which means that we make the boundary layers weak. In the outflow case we have:

Outflow criterion for weak boundary layers. The outflow boundary layers in the fundamental solution (6) are weak if α_u and α_v are small compared to α_1.

5. APPLICATION OF BOUNDARY CONDITIONS AND THE SUPPRESSION OF THE BOUNDARY LAYERS

In this section we will apply boundary conditions for the inflow and the outflow cases. We will also see that solid wall and free surface conditions are special cases of inflow conditions. Both classical and new boundary conditions will be considered. We will investigate the strength of the boundary layers induced by the different boundary conditions. We will see that the new conditions result in weaker boundary layers than the classical ones. We need three boundary conditions, as we have three free parameters in the fundamental solution, namely α_1, α_u, and α_v.

5.1. Inflow

The Boundary Condition

As inflow boundary conditions we propose to prescribe values for u and $\partial^r v/\partial x^r$ and to let $u_x + v_y = 0$. However, in order to see how errors in the boundary condition influence the solution, we let the divergence be non-zero at the boundary. Hence, we prescribe

$$\begin{pmatrix} u \\ \dfrac{\partial^r v}{\partial x^r} \\ u_x + v_y \end{pmatrix}(0, y, t) = \begin{pmatrix} u_0 \\ v_0^r \\ d_0 \end{pmatrix}(y, t), \qquad r = 0 \text{ or } 1 \text{ or } 2. \tag{10}$$

We will later prove that the higher value of r we choose, the more the inflow boundary layer will be suppressed. However, choosing $r \geqslant 3$ will give solutions that grow in time, even if the forcing function does not. We recommend using $r = 2$.

Naughton, [6], proposed prescribing u, v, and u_x at $x = 0$, i.e., (10) with $r = 0$. He used the energy method to prove stability for this boundary condition. Naughton also proposed prescribing values for v, u_x, and $p + \gamma u$, $\gamma \geqslant U/2$, and recommended using $\gamma = U$. Hence, we recommend using a higher order x-derivative than Naughton did.

The no-slip condition $u = v = 0$ at $x = 0$, together with the condition $u_x + v_y = 0$ at $x = 0$, can be found from (10) by letting $r = 0$ and $u_0 \equiv v_0^0 \equiv d_0 \equiv 0$. Hence, the case $r = 0$ can also be used for the case of a solid wall.

For $r = 1$ and $u_0 \equiv v_0^r \equiv d_0 \equiv 0$ we obtain a boundary condition which means that no fluid passes the boundary ($u = 0$ at $x = 0$) and that there is no shear stress at the boundary ($v_x = 0$ at $x = 0$). Hence, the case $r = 1$ can also be used for a free surface which is fixed at $x = 0$.

The Solution on the Laplace–Fourier Transform Side

Applying the Laplace–Fourier transform of the boundary condition (10) to the fundamental solution (6) and (7) yields

$$\begin{aligned}
\begin{pmatrix} \hat{u} \\ \hat{v} \\ \hat{p} \end{pmatrix} = {} & \frac{|\omega|/\omega}{\kappa_2^{r+1} - |\omega|^{r+1}} \left\{ \begin{pmatrix} \dfrac{|\omega|}{\omega}\kappa_2^{r+1} \\ -i\cdot\kappa_2^{r+1} \\ -\dfrac{-s + U\cdot|\omega| - i\omega V}{\omega}\kappa_2^{r+1} \end{pmatrix} \cdot e^{-|\omega|x} \right. \\
& \left. + \begin{pmatrix} -\omega\cdot|\omega|^r \\ i\kappa_2|\omega|^r \\ 0 \end{pmatrix} e^{-\kappa_2 x} \right\} \cdot \hat{u}_0 \\
& + \frac{(-1)^{r+1}}{\kappa_2^{r+1} - |\omega|^{r+1}} \left\{ \begin{pmatrix} i\omega \\ |\omega| \\ -\dfrac{-s + U\cdot|\omega| - i\omega V}{\omega} i|\omega| \end{pmatrix} \cdot e^{-|\omega|x} \right. \\
& \left. + \begin{pmatrix} -i\omega \\ -\kappa_2 \\ 0 \end{pmatrix} \cdot e^{-\kappa_2 x} \right\} \cdot \hat{v}_0^r \\
& + \frac{|\omega|/\omega}{\kappa_2^{r+1} - |\omega|^{r+1}} \left\{ \begin{pmatrix} \dfrac{|\omega|}{\omega}\kappa_2^r \\ -i\cdot\kappa_2^r \\ -\dfrac{-s + U\cdot|\omega| - i\omega V}{\omega}\kappa_2^r \end{pmatrix} \cdot e^{-|\omega|x} \right. \\
& \left. + \begin{pmatrix} -\dfrac{|\omega|}{\omega}\kappa_2^r \\ i|\omega|^r \\ 0 \end{pmatrix} \cdot e^{-\kappa_2 x} \right\} \cdot \hat{d}_0,
\end{aligned} \tag{11}$$

for $\text{Real}(s) > -\nu\omega^2$ and $s \neq U|\omega| - i\omega V$ and

$$\begin{pmatrix} \hat{u} \\ \hat{v} \\ \hat{p} \end{pmatrix} = \begin{pmatrix} \hat{u}_0 \\ -i\dfrac{|\omega|}{\omega}\dfrac{r\,\hat{u}_0}{r+1} + \dfrac{\hat{v}_0^r}{(r+1)(-|\omega|)^r} + \dfrac{r\,\hat{d}_0}{i\omega(r+1)} \\ \dfrac{2\nu|\omega|+U}{r+1}\left(\hat{u}_0 + \dfrac{i\omega\,\hat{v}_0^r}{(-|\omega|)^{r+1}} + \dfrac{\hat{d}_0}{|\omega|}\right) \end{pmatrix} \cdot e^{-|\omega|x}$$

$$+\frac{1}{r+1}\left(\hat{u}_0 + \frac{i\omega\,\hat{v}_0^r}{(-|\omega|)^{r+1}} + \frac{\hat{d}_0}{|\omega|}\right) \cdot x \cdot \begin{pmatrix} |\omega| \\ -i\omega \\ 0 \end{pmatrix} \cdot e^{-|\omega|x}, \qquad (12)$$

for $\text{Real}(s) > -\nu\omega^2$ and $s = U|\omega| - i\omega V$.

The solution defined by (11) and (12) is analytic at $s = U|\omega| - i\omega V$. Indeed, from (8.b) we have $\kappa_2 = |\omega| + k$ for $s = |\omega| U - i\omega V + k(2\nu|\omega| + U) + k^2\nu$. Continuity with respect to s is proven by substituting this into (11) and by letting $k \to 0$. From Ahlfors [1], Chap. 4, Section 3.1, it follows that the solution is analytic at $s = |\omega| U - i\omega V$.

The Analyticity of the Solution

By Lemma 3.1 we know that if we have a pole in the solution at $s = s_p$, $\text{Real}(s_p) > 0$, it means that the inverse Laplace–Fourier transformed solution will grow as $e^{\text{Real}(s_p)t}$, even if the forcing function does not grow at all. Therefore, we do not accept boundary conditions that lead to solutions with poles s_p with $\text{Real}(s_p) > 0$. We have the following theorem.

THEOREM 5.1. *Consider the solution* (11), (12) *to the problem* (5) *with the boundary condition at* $x = 0$ *taken to be the Laplace–Fourier transform of* (10). *For* $0 \leqslant r \leqslant 3$ *and* $U \geqslant 0$ *this solution is analytic for* $\text{Real}(s) \geqslant 0$. *Accordingly, the inverse Laplace–Fourier transform will have no exponentially growing solutions in time.*

Proof. As $\hat{u}_0$, $\hat{v}_0$, and $\hat{d}_0$ are analytic for all s, the only s with $\text{Real}(s) \geqslant 0$ where the solution (11), (12) might not be analytic are those s for which $\kappa_2^{r+1} = |\omega|^{r+1}$, that is,

$$\kappa_2 = |\omega| \cdot e^{i2\pi m/(r+1)}, \qquad 0 \leqslant m \leqslant r, \quad 0 \leqslant r \leqslant 3.$$

Together with (8.b) this implies that

$$s = -\omega^2\nu(1 - e^{i2\pi 2m/(r+1)}) + U|\omega| \cdot e^{i2\pi m/(r+1)} - i\omega V,$$
$$0 \leqslant m \leqslant r, \quad 0 \leqslant r \leqslant 3. \qquad (13)$$

All the s in (13) have negative real part, except $s = |\omega| U - i\omega V$ (which is attained for $m = 0$). However, as pointed out just after (12), the solution is analytic at $s = |\omega| U - i\omega V$, which proves Theorem 5.1. ∎

Note that using $r = 3$ is bad in case we have $\nu \ll 1$. This is because two poles ($m = 1$ and $m = 3$) will approach the imaginary axis when $\nu \to 0$. The damping in the system is then weak, and for more general spatial differential operators than the one derived by linearizing around a constant flow, or for the two-point boundary value problem, the solution might grow, even if g does not, [2]. According to the next theorem, the case $r \geqslant 4$ will give solutions that grow very fast in time.

THEOREM 5.2. *Consider the solution* (11), (12) *to the problem* (5) *with the boundary conditions at* $x = 0$ *taken to be the Laplacian–Fourier transform of* (10). *Let* $r \geqslant 4$ *and* $U > 0$. *For large* t *the inverse transformed solution will grow as* $\exp(K(r)\,U^2 t/\nu)$, *where* $K > 0$.

Proof. Letting $m = 1$ in (13) yields

$$s_p = -\omega^2\nu(1 - e^{i2\pi 2/(r+1)}) + U|\omega| \cdot e^{i2\pi/(r+1)} - i\omega V,$$

which together with (8.b) gives $\kappa_2 = |\omega| \cdot e^{i2\pi/(r+1)}$. Hence, if $\text{Real}(s_p) > -\nu\omega^2$, then the solution (11) has a pole of order one at $s = s_p$. For

$$\omega = \text{Int}\left[\frac{U \cdot \text{Real}(e^{i2\pi/(r+1)})}{2\nu\,\text{Real}(1 - e^{i2\pi 2/(r+1)})}\right]$$

we as $r \geqslant 4$ obtain

$$\text{Real}(s_p) = \frac{U^2 \cdot (\text{Real}(e^{i2\pi/(r+1)}))^2}{4\nu\,\text{Real}(1 - e^{i2\pi 2/(r+1)})} + O(1)$$

$$= \frac{1}{8}\cot^2\left(\frac{2\pi}{r+1}\right) \cdot \frac{U^2}{\nu} + O(1) > 0.$$

According to Lemma 3.1 this means that the solution on the inverse transform side will approximately grow as $\exp(\frac{1}{8}\cot^2(2\pi/(r+1)) \cdot (U^2/\nu)t)$. The proof of Theorem 5.2 is complete. ∎

The Divergence

From (11), (12) we see that

$$\hat{u}_x + i\omega\hat{v} = \hat{d}_0 e^{-\kappa_2 x}.$$

Hence, we make the solution divergence free by letting $\hat{d}_0 = 0$. Also note that if $\nu \ll U/|\omega|$ and if $\nu \ll U^2/|s|$, we obtain $\kappa_2 \approx \nu\omega^2/U \ll |\omega|$, according Section 4.2. Therefore, if we let $\hat{d}_0 \neq 0$, the divergence will in this case not be confined to the boundary.

The Strength of the Boundary Layer

Again we have from Section 4.2 that if $\nu \ll U/|\omega|$ and if $\nu \ll U^2/|s|$, we obtain $\kappa_2 \approx \nu\omega^2/U \ll |\omega|$. The fundamental solution will in this case contain a boundary layer. This layer is weak if α_1 is small compared to α_u and α_v.

For simplicity let $\hat{d}_0 = \hat{v}_0^r = 0$. From (6) and (11) we see that

$$\left|\frac{\alpha_1}{\alpha_u}\right| = \left|\frac{\kappa_2}{\omega}\right|^{r+1} \approx \left|\frac{\nu\omega}{U}\right|^{r+1} \ll 1 \tag{14.a}$$

$$\left|\frac{\alpha_1}{\alpha_v}\right| = \left|\frac{\kappa_2}{\omega}\right|^{r} \approx \left|\frac{\nu\omega}{U}\right|^{r} \ll 1, \qquad \text{if} \quad r \leqslant 1. \tag{14.b}$$

We conclude that increasing r in (1), i.e., the order of the x-derivative of v, results in weaker boundary layer at the inflow.

5.2. Outflow

The Boundary Condition

As in the inflow case, we will try to avoid boundary layers. From Section 4.2 we remember that in the outflow case, small ν makes $|\kappa_2| \gg |\omega|$. This is the opposite situation from the inflow case. In order to avoid boundary layers we want the coefficients α_u and α_v to be small compared to α_1. This is done by prescribing an x-derivative of high order of u and v to be zero. However, in order to see how errors in the boundary condition influence the solution, we will here let those derivatives be non-zero at the boundary. As the third condition, we prescribe the pressure. Hence, give as the boundary condition

$$\begin{pmatrix} \dfrac{\partial^j u}{\partial x^j} \\ \dfrac{\partial^q v}{\partial x^q} \\ p \end{pmatrix} (0, y, t) = \begin{pmatrix} u_0^j \\ v_0^q \\ p_0 \end{pmatrix} (y, t). \tag{15}$$

We will later prove that the choice $j = q + 1$, together with $u_0^j = v_0^q = 0$, will guarantee the solution to be divergence free in the entire domain. Furthermore, the higher value of j and q we choose, the more the outflow boundary layers will be suppressed.

Naughton, [6], proposed two different boundary conditions. The first was to prescribe u_x, v_x, and p, and the second was to prescribe u_{xx}, v_x, and $p + \gamma u - \nu u_x$, $\gamma \geqslant U/2$. He recommended using $\gamma = 0$. We will later see that in the first condition that Naughton used, the divergence does not vanish. Furthermore, we will see that the outflow boundary layers are not efficiently suppressed.

We recommend using $j = 3$ and $q = 2$ in (15). In case the viscosity is small, we can also use $j = 2$ and $q = 2$. Hence, as in the inflow case we again recommend using a higher order x-derivative than Naughton did.

The Solution on the Laplace–Fourier Transform Side

Applying the Laplace–Fourier transform of the boundary condition (15) to the fundamental solution (6) and (7) yields

$$\begin{aligned} \begin{pmatrix} \hat{u} \\ \hat{v} \\ \hat{p} \end{pmatrix} &= \begin{pmatrix} \dfrac{1}{(-\kappa_2)^j} \\ 0 \\ 0 \end{pmatrix} \cdot e^{-\kappa_2 x} \hat{u}_0^j \\ &+ \begin{pmatrix} 0 \\ \dfrac{1}{(-\kappa_2)^q} \\ 0 \end{pmatrix} \cdot e^{-\kappa_2 x} \hat{v}_0^q \\ &+ \frac{\omega}{s - U \cdot |\omega| + i\omega V} \left\{ \begin{pmatrix} \dfrac{|\omega|}{\omega} \\ -i \\ \dfrac{s - U \cdot |\omega| + i\omega V}{\omega} \end{pmatrix} \cdot e^{-|\omega| x} \right. \\ &\left. + \begin{pmatrix} -\dfrac{|\omega|}{\omega} \left(\dfrac{|\omega|}{\kappa_2}\right)^j \\ i \left(\dfrac{|\omega|}{\kappa_2}\right)^q \\ 0 \end{pmatrix} \cdot e^{-\kappa_2 x} \right\} \cdot \hat{p}_0 \end{aligned} \tag{16}$$

for $\text{Real}(s) > -\nu\omega^2$ and $s \neq |\omega|\, U - i\omega V$ and

$$\begin{aligned} \begin{pmatrix} \hat{u} \\ \hat{v} \\ \hat{p} \end{pmatrix} &= \begin{pmatrix} \dfrac{j \cdot \hat{p}_0}{2\nu\,|\omega| + U} + \dfrac{\hat{u}_0^j}{(-|\omega|)^j} \\ -i \cdot \dfrac{|\omega|}{\omega} \dfrac{q \cdot \hat{p}_0}{2\nu\,|\omega| + U} + \dfrac{\hat{v}_0^q}{(-|\omega|)^q} \\ \hat{p}_0 \end{pmatrix} \cdot e^{-|\omega| x} \\ &+ \frac{|\omega|}{2\nu\,|\omega| + U} \begin{pmatrix} 1 \\ -i\dfrac{|\omega|}{\omega} \\ 0 \end{pmatrix} \cdot x \cdot e^{-|\omega| x} \cdot \hat{p}_0 \end{aligned} \tag{17}$$

for $\text{Real}(s) > -\nu\omega^2$ and $s = U\,|\omega| - i\omega V$.

The solution (16), (17) is analytic at $s = U\,|\omega| - i\omega V$ for $\text{Real}(s) > -\nu\omega^2$. This is proven in the same way as for the inflow case.

The Analyticity of the Solution

THEOREM 5.3. *Consider the solution* (16), (17), *valid for* $\text{Real}(s) > -\nu\omega^2$, *to the problem* (5) *with the boundary condition at* $x=0$ *taken to be the Laplace–Fourier transform of* (15). *This solution is analytic for* $\text{Real}(s) > -\nu\omega^2$.

Proof. We have already seen that (16), (17) is analytic at $s = U|\omega| - i\omega V$. Therefore, the only s with $\text{Real}(s) > -\nu\omega^2$, where the solution (16), (17) might not be analytic are those s for which $\kappa_2 = 0$. By (8.b) we obtain $\kappa_2 = 0$ for $s = -\nu\omega^2 - i\omega V$, and the theorem is proven. ∎

The Divergence

From (16) we see that

$$\hat{u}_x + i\omega\hat{v} = \left\{ \frac{\hat{u}_0^j}{(-\kappa_2)^{j-1}} + \frac{i\omega\cdot\hat{v}_0^q}{(-\kappa_2)^q} + \frac{\omega^2\cdot\hat{p}_0}{s - U|\omega| + i\omega V} \times \left(\left(\frac{|\omega|}{\kappa_2}\right)^{j-1} - \left(\frac{|\omega|}{\kappa_2}\right)^q \right) \right\} \cdot e^{-\kappa_2 x}.$$

Hence, we make the solution divergence free by letting $\hat{u}_0^j = \hat{v}_0^q = 0$ and by choosing $j = q+1$, that is, by giving one order higher x-derivative of u than of v.

If the requirement $j = q+1$ is not fulfilled, the divergence will not vanish. However, if $\text{Real}(\kappa_2) \gg |\omega|$, for instance if $\nu \ll |U|/|\omega|$, then the divergence will be confined to a boundary layer at the outflow boundary. In this case it is not very important to have the requirement $j = q+1$ fulfilled, as long as we make the boundary layers weak by choosing j and q large. This will be illustrated in Section 6.

The Strength of the Boundary Layer

From Section 4.2 we remember that if $\nu \ll |U|/|\omega|$ we obtain $\text{Real}(\kappa_2) \gg |\omega|$. The fundamental solution will in this case contain a boundary layer. This layer is weak if α_u and α_v are small compared to α_1.

For simplicity let $\hat{u}_0^j = \hat{v}_0^q = 0$. From (6) and (16) we obtain

$$\left|\frac{\alpha_u}{\alpha_1}\right| = \left|\frac{\omega}{\kappa_2}\right|^j \ll 1, \quad \text{if} \quad j \geq 1, \tag{18.a}$$

$$\left|\frac{\alpha_v}{\alpha_1}\right| = \left|\frac{\omega}{\kappa_2}\right|^q \ll 1, \quad \text{if} \quad q \geq 1. \tag{18.b}$$

To suppress boundary layers we must choose $j \geq 1$ and $q \geq 1$. The larger we choose j and q, the more the boundary layers will be suppressed.

6. THE NUMERICAL SOLUTION OF THE NON-LINEAR PROBLEM

In this section we show numerical results for the non-linear Navier–Stokes equation (3). It turns out that the analytical results in Sections 2–5 concerning boundary layers and divergence in the solution of the linearized equations hold true for the non-linear equations as well. In Section 6 we use the notation u, v, p both for the solution of the linearized equation and for the solution of the non-linear equation. What is meant in every case will be clear from the context.

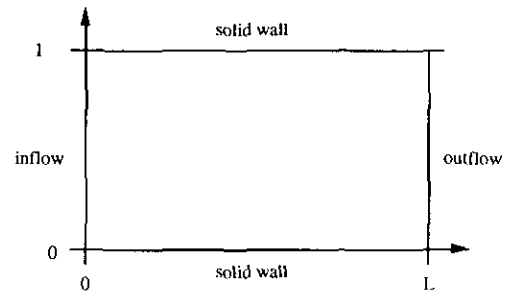

FIG. 1. The calculation domain.

6.1. The Numerical Method

We have written a code for solving the time-dependent, incompressible, non-linear Navier–Stokes equation (3) in $0 \leq x \leq L$, $0 \leq y \leq 1$, $0 \leq t < \infty$, i.e., a two-dimensional straight channel. All the spatial derivatives in (3.a), (3.b) and the first-order derivatives in (3.c) are approximated by the standard fourth-order central differences on a Cartesian grid. This means that the differential operators $\partial/\partial x$, $\partial/\partial y$, and $\partial^2/\partial x^2 + \partial^2/\partial y^2$ are exchanged for finite difference operators according to

$$\frac{\partial}{\partial x} \to D_{0x}\left(I - \frac{\Delta x^2}{6} D_{+x}D_{-x}\right)$$

$$\frac{\partial}{\partial y} \to D_{0y}\left(I - \frac{\Delta y^2}{6} D_{+y}D_{-y}\right)$$

$$\frac{\partial^2}{\partial x^2} + \frac{\partial^2}{\partial y^2} \to D_{+x}D_{-x}\left(I - \frac{\Delta x^2}{12} D_{+x}D_{-x}\right) + D_{+y}D_{-y}\left(I - \frac{\Delta y^2}{12} D_{+y}D_{-y}\right).$$

Here D_{+x}, D_{-x}, D_{0x}, D_{+y}, D_{-y}, and D_{0y} are the forward, backward, and central difference operators, e.g., $D_{+x}u_{i,j} = (u_{i+1,j} - u_{i,j})/\Delta x$ and $D_{0y}u_{i,j} = (u_{i,j+1} - u_{i,j-1})/2\Delta y$. The Poisson equation (3.c) is solved by the fourth-order FISHPACK routine SEPELI. This routine solves the separable Poisson equation by a generalized cyclic reduction algorithm based on difference approximations [7].

As boundary conditions we apply (1) at $x = 0$ and (2) at $x = L$. At the solid walls we apply $u = v = u_x + v_y = 0$. As the spatial discretization is fourth-order accurate, we also need extra boundary conditions to have the method well defined, [2]. These extra conditions must be chosen in such a way

that the fourth-order accuracy of the method is not destroyed. How this is done will be discussed later.

As the initial condition we let $u(x, y, 0) = u(0, y, 0)$ and $v(x, y, 0) = p(x, y, 0) = 0$. Denote the so-derived approximation of the velocity $\binom{u}{v}(x_i, y_j, t)$ by $w_{i,j}(t)$ and the vector consisting of the $w_{i,j}$:s in all gridpoints (i, j) by $\mathbf{w}$. For the pressure we use the notations $p_{i,j}(t)$ and $\mathbf{p}$. The method of lines approximation of (3) can then be written as

$$\mathbf{w}_t = F(\mathbf{w}, \mathbf{p}) \tag{19.a}$$

$$L(\mathbf{p}) = G(\mathbf{w}), \tag{19.b}$$

where F is the approximation of the convective and viscous terms and of the pressure gradient in (3.a), (3.b), L is the approximation of the Laplace operator in (3.c), and G is the approximation of the rest of (3.c). Equation (19) is a system of differential algebraic equations (DAE). We solve it by integrating in time with the fourth-order standard Runge–Kutta method. The Poisson equation is solved in every intermediate step, that is, four times for every Runge–Kutta step. Hence, the system (19) is integrated by

$$\begin{aligned}
&\mathbf{k}_1 := \Delta t \cdot F(\mathbf{w}^n, \mathbf{p}^n), && \mathbf{w}_1 := \mathbf{w}^n + \tfrac{1}{2}\mathbf{k}_1,\\
&\mathbf{p}_1 := L^{-1}(G(\mathbf{w}_1))\\
&\mathbf{k}_2 := \Delta t \cdot F(\mathbf{w}_1, \mathbf{p}_1), && \mathbf{w}_2 := \mathbf{w}^n + \tfrac{1}{2}\mathbf{k}_2,\\
&\mathbf{p}_2 := L^{-1}(G(\mathbf{w}_2))\\
&\mathbf{k}_3 := \Delta t \cdot F(\mathbf{w}_2, \mathbf{p}_2), && \mathbf{w}_3 := \mathbf{w}^n + \mathbf{k}_3,\\
&\mathbf{p}_3 := L^{-1}(G(\mathbf{w}_3))\\
&\mathbf{k}_4 := \Delta t \cdot F(\mathbf{w}_3, \mathbf{p}_3),\\
&\mathbf{w}^{n+1} := \mathbf{w}^n + \tfrac{1}{6}(\mathbf{k}_1 + 2\mathbf{k}_2 + 2\mathbf{k}_3 + \mathbf{k}_4),\\
&\mathbf{p}^{n+1} := L^{-1}(G(\mathbf{w}^{n+1})).
\end{aligned}$$

The time step is chosen so that the fourth-order accurate Cauchy problem

$$\begin{aligned}
u_t &+ U \cdot D_{0x}\left(I - \frac{\Delta x^2}{6} D_{+x}D_{-x}\right)u\\
&+ V \cdot D_{0y}\left(I - \frac{\Delta y^2}{6} D_{+y}D_{-y}\right)u\\
&= \nu\left\{D_{+x}D_{-x}\left(I - \frac{\Delta x^2}{12} D_{+x}D_{-x}\right)\right.\\
&\left. + D_{+y}D_{-y}\left(I - \frac{\Delta y^2}{12} D_{+y}D_{-y}\right)\right\}u
\end{aligned}$$

is stable. The pressure gradient in the full equations acts as lower order velocity terms, which we neglect. Taking the discrete Fourier transform of the above equation yields

$$\begin{aligned}
&\bar{u}_t = \lambda\bar{u},\\
&\lambda = -\frac{iU}{\Delta x}\sin(\alpha)\left(1 + \frac{2}{3}\sin^2(\alpha/2)\right)\\
&\quad - \frac{iV}{\Delta y}\sin(\beta)\left(1 + \frac{2}{3}\sin^2(\beta/2)\right)\\
&\quad - \frac{4\nu}{\Delta x^2}\sin^2(\alpha/2)\left(1 + \frac{1}{3}\sin^2(\alpha/2)\right)\\
&\quad - \frac{4\nu}{\Delta y^2}\sin^2(\beta/2)\left(1 + \frac{1}{3}\sin^2(\beta/2)\right),
\end{aligned}$$

where $\alpha = \omega_x \Delta x$, $\beta = \omega_y \Delta y$, $-\pi \leqslant \alpha \leqslant \pi$, and $-\pi \leqslant \beta \leqslant \pi$.

It is easily found that $\max_\alpha |\sin(\alpha)(1 + \frac{2}{3}\sin^2(\alpha/2))| \approx 1.372$, i.e., $|\mathrm{Im}(\lambda)| \leqslant 1.372 \cdot (|U|/\Delta x + |V|/\Delta y)$. Furthermore, $-(16\nu/3)(1/\Delta x^2 + 1/\Delta y^2) \leqslant \mathrm{Real}(\lambda) \leqslant 0$. Choosing the time step such that

$$1.372 \cdot \left(\frac{|U|}{\Delta x} + \frac{|V|}{\Delta y}\right) \cdot i \cdot \Delta t - \frac{16\nu}{3}\left(\frac{1}{\Delta x^2} + \frac{1}{\Delta y^2}\right) \cdot \Delta t$$

is in the stability region of the Runge–Kutta method makes the above fourth-order accurate Cauchy problem stable. We therefore choose the time step for Eq. (19) to this value as well. In the following we will in detail discuss how to choose the extra boundary conditions.

The Numerical Treatment of the Boundaries

The numerical boundary conditions have to be accurate enough to keep the fourth-order accuracy for all x [2]. In order to understand how boudaries should be treated numerically when using a fourth-order spatial approximation we start by treating a simple model problem. Therefore, consider the problem

$$u_t = u_{xx} \qquad 0 \leqslant t < \infty, \quad 0 \leqslant x < \infty, \tag{20.a}$$

$$u(x, 0) = 0, \qquad 0 \leqslant x < \infty, \tag{20.b}$$

$$u(0, t) = g(t), \qquad 0 \leqslant t, \tag{20.c}$$

$$\int_0^\infty e^{-2\eta t}\,\|u(\cdot, t)\|^2\,dt < \infty, \qquad \eta > \eta_0. \tag{20.d}$$

Consider the numerical approximation $u_j(t) \approx u(x_j, t)$ on the grid $x_j = h \cdot j$ for $j = -1, 0, 1, 2, \ldots$, where u_j is defined by

$$u_{j,t} = D_+ D_- \left(I - \frac{h^2}{12} D_+ D_-\right) u_j,$$

$$0 \leqslant t < \infty, \quad j = 1, 2, 3, \ldots, \tag{21.a}$$

$$u_j(0) = 0, \qquad j = -1, 0, 1, 2, \ldots, \tag{21.b}$$

$$u_0(t) = g(t), \quad B_E u_0(t) = 0, \qquad 0 \leqslant t, \tag{21.c}$$

$$\int_0^\infty e^{-2\eta t}\,\|u.(t)\|_h^2\,dt < \infty, \qquad \eta > \eta_0, \tag{21.d}$$

where $\|u.(t)\|_h^2 = \sum_{j=-1}^{\infty} |u_j(t)|^2 h$. We note that as the fourth-order accurate operator $D_+ D_-(I-(h^2/12) D_+ D_-)$ is a five-point operator, we need two boundary conditions at $j=0$. The first one, $u_0(t)=g(t)$, is taken from (20.c). The aim of the investigation that follows is to determine the extra boundary condition $B_E u_0(t)=0$ in such a way that (21) is a fourth-order accurate approximation of (20).

Before going further with the solution of (21) we will prove a simple lemma that tells that if a method is fourth-order accurate on the time side, then it is fourth-order accurate on the Laplace transform side.

LEMMA 6.1. *Consider the functions*

$$u=u(x,t), \qquad 0\leqslant x<\infty, \quad 0\leqslant t<\infty$$

and

$$u_j=u_j(t,h), \qquad j=0,1,2,..., \quad 0\leqslant t<\infty, \quad 0<h\leqslant h_0.$$

Let $x_j = h\cdot j$ and assume that for some $\alpha\in R$ and for some integer $q\geqslant 1$,

$$|u(x,t)|<f(x)\cdot e^{\alpha t}$$

and

$$|u(x_j,t)-u_j(t,h)|<h^q\cdot f(x_j)\cdot e^{\alpha t}.$$

Then

$$|\tilde{u}(x_j,s)-\tilde{u}_j(s,h)|<\frac{f(x_j)}{\text{Real}(s)-\alpha}\cdot h^q, \qquad \text{Real}(s)>\alpha.$$

Proof. The Laplace transforms are well defined for $\text{Real}(s)>\alpha$ and

$$\left|\int_0^\infty e^{-st}(u(x_j,t)-u_j(t,h))\,dt\right| < \int_0^\infty e^{-\text{Real}(s)t}\cdot h^q\cdot f(x_j)\cdot e^{\alpha t}\,dt=\frac{f(x_j)}{\text{Real}(s)-\alpha}\cdot h^q. \quad \blacksquare$$

For $\text{Real}(s)>0$ the Laplace transform of the solution of (20) is

$$\tilde{u}(x,s)=\tilde{g}(s)\,e^{-\sqrt{s}x},$$

where the root sign means the branch with positive real part. The fundamental solution of the Laplace transform of (21) is (see [2] for details)

$$\tilde{u}_j(s)=\alpha_t(s)\cdot e^{-\kappa_t x_j}+\alpha_f(s)\cdot e^{-\kappa_f x_j}, \tag{22.a}$$

where

$$\kappa_t=\frac{2}{h}\sinh^{-1}\left[\left(\frac{3}{2}-\frac{3}{2}\left(1-\frac{sh^2}{3}\right)^{1/2}\right)^{1/2}\right] = s^{1/2}\cdot\{1+O(s^2h^4)\}, \tag{22.b}$$

$$\kappa_f=\frac{2}{h}\sinh^{-1}\left[\left(\frac{3}{2}+\frac{3}{2}\left(1-\frac{sh^2}{3}\right)^{1/2}\right)^{1/2}\right] =\frac{2}{h}\sinh^{-1}(3^{1/2})\cdot\{1+O(sh^2)\}, \tag{22.c}$$

The indices t and f stand for true and false. Note that κ_t approximates the correct value $s^{1/2}$. Furthermore, $e^{-\kappa_f x_j}$ is the parasite solution representing a boundary layer with the thickness of the grid size h. This part of the fundamental solution (22.a) occurs because we use a fourth-order accurate approximation in (21.a).

We will now show how the fourth-order accuracy on the Laplace transform side can be investigated for our model problem. If we in (22.a) had $\alpha_t=\tilde{g}$ and $\alpha_f=0$ we, for every fixed x_j and fixed s, would have the error $|\tilde{u}_j(s)-\tilde{u}(x_j,s)| = |\{\exp(O(s^2h^4)\cdot s^{1/2}\cdot x_j)-1\}\cdot\tilde{g}(s)\,e^{-\sqrt{s}x_j}| = O(h^4)$. The method would for every fixed s and x be fourth-order accurate on the Laplace transform side. Hence, the role the extra boundary condition $B_E u_0(t)=0$ must play is to eliminate the parasite solution $\alpha_f(s)\cdot e^{-\kappa_f x_j}$.

In order to illustrate how well different B_E eliminate the parasite solution we will try three B_E's namely

$$D_+ D_- u_0=0 \Leftrightarrow D_+ D_-\tilde{u}_0=0, \tag{23.a}$$

$$D_+^3 D_- u_0=0 \Leftrightarrow D_+^3 D_-\tilde{u}_0=0, \tag{23.b}$$

and

$$\frac{\partial u_0}{\partial t}=D_+ D_- u_0 \Leftrightarrow s\tilde{u}_0=D_+ D_-\tilde{u}_0. \tag{23.c}$$

From the fundamental solution (22.a), together with the Laplace transform of the boundary condition (21.c), where the extra condition is chosen to be (23.a), we obtain

$$\alpha_t=\frac{\tilde{g}}{1-\dfrac{\sinh^2(\kappa_t h/2)}{\sinh^2(\kappa_f h/2)}} =\frac{\tilde{g}}{1-\dfrac{1-(1-sh^2/3)^{1/2}}{1+(1-sh^2/3)^{1/2}}}=\tilde{g}\cdot\{1+O(sh^2)\},$$

$$\alpha_f=\tilde{g}\cdot O(sh^2),$$

and the method is only second-order accurate on the

Laplace transform side. Hence, using (23.a) as the extra boundary condition in (21.c) will, according to Lemma 6.1, destroy the fourth-order accuracy.

A similar calculation shows that in both cases (23.b) and (23.c) we obtain

$$\alpha_t = \tilde{g} \cdot \{1 + O(s^2h^4)\}$$
$$\alpha_f = \tilde{g} \cdot O(s^2h^4)$$

and the relative error is $O(s^2h^4)$, so the approximation is, for every fixed s and x, fourth-order accurate on the Laplace transform side.

In the boundary condition (23.b) we need five grid points to obtain fourth-order accuracy, namely, $j = -1, 0, 1, 2, 3$. In the condition (23.c) we derive fourth-order accuracy with only three grid points involved, namely, $j = -1, 0, 1$. This is so because we use the differential equation to construct the extra boundary condition. From this we learn that using the differential equation when constructing the extra boundary condition will reduce the needed number of grid points.

Instead of the problem (20) we now consider the more realistic problem (4) with $U = V = 0$ and $\nu = 1$. As an example, we at $x = 0$ will apply the boundary condition (1) with $r = 0$ and $v_0^r = 0$. We let u_j, v_j, p_j be the numerical approximation on the grid $x_j = h \cdot j$, $j = -1, 0, 1, 2, \ldots$. We approximate the x-derivatives with fourth-order finite differences and take the Laplace–Fourier transform in time and the y-direction. We let $\hat{u}_j$, $\hat{v}_j$, and $\hat{p}_j$ be the Laplace–Fourier transforms of u_j, v_j, and p_j. We obtain the system

$$su_j - D_+D_-\left(I - \frac{h^2}{12}D_+D_-\right)\hat{u}_j + \omega^2\hat{u}_j + D_0\left(I - \frac{h^2}{6}D_+D_-\right)\hat{p}_j = 0,$$
$$j = 1, 2, 3, \ldots, \quad \omega = \pm 1, \pm 2, \ldots, \tag{24a}$$

$$s\hat{v}_j - D_+D_-\left(I - \frac{h^2}{12}D_+D_-\right)\hat{v}_j + \omega^2\hat{v}_j + i\omega\hat{p}_j = 0,$$
$$j = 1, 2, 3, \ldots, \quad \omega = \pm 1, \pm 2, \ldots, \tag{24b}$$

$$D_+D_-\left(I - \frac{h^2}{12}D_+D_-\right)\hat{p}_j - \omega^2\hat{p}_j = 0,$$
$$j = 1, 2, 3, \ldots, \quad \omega = \pm 1, \pm 2, \ldots, \tag{24c}$$

$$\hat{u}_0 = \hat{g}_u(\omega, s), \qquad \hat{v}_0 = 0, \qquad D_x^{(4)}\hat{u}_0 + i\omega\hat{v}_0 = 0,$$
$$\omega = \pm 1, \pm 2, \ldots, \tag{24d}$$

$$\int_{-\infty}^{\infty} (\|\hat{u}.(\cdot, \eta + i\xi)\|_h^2 + \|\hat{v}.(\cdot, \eta + i\xi)\|_h^2 + \|\hat{p}.(\cdot, \eta + i\xi)\|_h^2)\, d\xi < \infty, \qquad \eta > \eta_0. \tag{24e}$$

The operator $D_x^{(4)}$, that approximates $\partial/\partial x$ to the fourth order in the boundary condition (24.d), can for instance be defined by $D_x^{(4)}\hat{u}_0 = (-3\hat{u}_{-1} - 10\hat{u}_0 + 18\hat{u}_1 - 6\hat{u}_2 + \hat{u}_3)/12h$. Note that we have not yet specified the three extra boundary conditions needed to eliminate the parasite solution.

The fundamental solution of the system (24.a)–(24.c), (24.e) is

$$\begin{aligned}\begin{pmatrix}\hat{u}\\ \hat{v}\\ \hat{p}\end{pmatrix}_j(\omega, s) = {} & \alpha_{1t} \cdot \begin{pmatrix} \dfrac{|\omega|}{\omega} + O(\omega^4h^4) \\ -i \\ \dfrac{s}{\omega}\end{pmatrix} \cdot e^{-\kappa_{1t}x_j} \\ & + \alpha_{ut} \cdot \begin{pmatrix}1\\0\\0\end{pmatrix} \cdot e^{-\kappa_{2t}x_j} + \alpha_{vt} \cdot \begin{pmatrix}0\\1\\0\end{pmatrix} \cdot e^{-\kappa_{2t}x_j} \\ & + h \cdot \alpha_{1f} \cdot \begin{pmatrix} 1 + O(\omega^2h^2) \\ \dfrac{i\omega h}{48^{1/2}} \\ -\dfrac{sh}{48^{1/2}}\end{pmatrix} \cdot e^{-\kappa_{1f}x_j} \\ & + h \cdot \alpha_{uf} \cdot \begin{pmatrix}1\\0\\0\end{pmatrix} \cdot e^{-\kappa_{2f}x_j} + \alpha_{vf} \cdot \begin{pmatrix}0\\1\\0\end{pmatrix} \cdot e^{-\kappa_{2f}x_j},\end{aligned} \tag{25.a}$$

where

$$\kappa_{1t} = \frac{2}{h}\sinh^{-1}\left[\left(\frac{3}{2} - \frac{3}{2}\left(1 - \frac{h^2\omega^2}{3}\right)^{1/2}\right)^{1/2}\right] = |\omega| \cdot \{1 + O(\omega^4h^4)\}, \tag{25.b}$$

$$\kappa_{2t} = \frac{2}{h}\sinh^{-1}\left[\left(\frac{3}{2} - \frac{3}{2}\left(1 - \frac{h^2(s+\omega^2)}{3}\right)^{1/2}\right)^{1/2}\right] = (s+\omega^2)^{1/2} \cdot \{1 + O((s+\omega^2)^2h^4)\}, \tag{25.c}$$

$$\kappa_{1f} = \frac{2}{h}\sinh^{-1}\left[\left(\frac{3}{2} + \frac{3}{2}\left(1 - \frac{h^2\omega^2}{3}\right)^{1/2}\right)^{1/2}\right] = \frac{2}{h}\sinh^{-1}(3^{1/2}) \cdot \{1 + O(\omega^2h^2)\}, \tag{25.d}$$

$$\kappa_{2f} = \frac{2}{h}\sinh^{-1}\left[\left(\frac{3}{2} + \frac{3}{2}\left(1 - \frac{h^2(s+\omega^2)}{3}\right)^{1/2}\right)^{1/2}\right] = \frac{2}{h}\sinh^{-1}(3^{1/2}) \cdot \{1 + O((s+\omega^2)h^2)\}. \tag{25.e}$$

The first three terms in (25.a) is a fourth-order accurate approximation of the fundamental solution (6), whereas the

last three terms is the parasitic solution with the boundary layer thickness h.

As in the previous simple model problem we will investigate how to choose the extra boundary conditions so that the parasite solution is eliminated. We saw in the former example that using the differential equation to construct the extra boundary conditions will reduce the needed number of grid points. We will follow the same idea and as extra boundary conditions use

$$u_{j,t} - D_{xx}^{(m_1)} u_j - u_{j,yy} + D_x^{(m_1)} p_j = 0, \qquad j = 0, \quad (26.a)$$

$$v_{j,t} - D_{xx}^{(m_2)} v_j - v_{j,yy} + p_{j,y} = 0, \qquad j = 0, \quad (26.b)$$

$$D_{xxx}^{(m_3)} p_j + D_x^{(m_3)} p_{j,yy} = 0, \qquad \text{or}$$

$$D_{xxxx}^{(m_4)} p_j + D_{xx}^{(m_4)} p_{j,yy} = 0, \qquad j = 0. \quad (26.c)$$

The finite difference operators are of order m_i; e.g., $D_{xx}^{(m_1)}$ approximates $\partial^2/\partial x^2$ to $O(h^{m_1})$ and $D_x^{(m_3)}$ approximates $\partial/\partial x$ to $O(h^{m_3})$.

Applying the boundary conditions (24.d), together with the Laplace–Fourier transform of the extra boundary conditions (26) to the fundamental solution (25) yields for every fixed ω and s a linear system of equations for the α's. By letting $m_1 \geq 3$, $m_2 \geq 2$, $m_3 \geq 3$, and $m_4 \geq 2$ and omitting all $O(h^4)$ terms in this system, a straightforward calculation yields the solution

$$\begin{pmatrix} \alpha_{1t} \\ \alpha_{ut} \\ \alpha_{vt} \end{pmatrix} = \frac{|\omega|}{\omega} \cdot \frac{1}{(s/\omega^2+1)^{1/2} - 1} \begin{pmatrix} (s/\omega^2+1)^{1/2} \\ -\dfrac{|\omega|}{\omega} \\ i(s/\omega^2+1)^{1/2} \end{pmatrix} \cdot \hat{g}_u, \quad (27.a)$$

$$\begin{pmatrix} \alpha_{1f} \\ \alpha_{uf} \\ \alpha_{vf} \end{pmatrix} = \begin{pmatrix} 0 \\ 0 \\ 0 \end{pmatrix} \quad (27.b)$$

(see [2] for details). Taking the $O(h^4)$ terms into account will only perturb the solution (27) with $O(h^4)$ terms. If we substitute the perturbed α's into the fundamental solution (25), we derive a fourth-order accurate approximation of the solution (11) with $r = 0$ and $\hat{v}_0^r = \hat{d}_0^r = 0$. Hence, the method is, for every fixed ω and s, fourth-order accurate on the Laplace–Fourier transform side if $m_1 \geq 3$, $m_2 \geq 2$, $m_3 \geq 3$, and $m_4 \geq 2$.

We have above described the procedure of how to define the extra boundary conditions so that the parasite solution is eliminated. As an example, we have investigated the inflow condition (1) with $r = 0$ in detail. For $r = 1$ and $r = 2$ and for the outflow condition (2) the procedure is similar. We have not proved stability for our fourth-order method theoretically. However, numerical experiments show that all the proposed boundary conditions give stable numerical schemes.

Numerical Verification of the Fourth-Order Spatial Accuracy

Lemma 6.1 gives a necessary but not sufficient condition for how to choose the extra boundary conditions such that the method becomes fourth-order accurate on the time side. Therefore the fourth-order accuracy in the space variables has also been checked numerically for steady state solutions. This is done by introducing forcing functions in the equations. Hence, we numerically solve

$$u_t + uu_x + vu_y - \nu u_{xx} - \nu u_{yy} + p_x = F_1,$$
$$0 \leq x \leq L, \quad 0 \leq y \leq 1, \quad 0 \leq t < \infty, \quad (28.a)$$

$$v_t + uv_x + vv_y - \nu v_{xx} - \nu v_{yy} + p_y = F_2,$$
$$0 \leq x \leq L, \quad 0 \leq y \leq 1, \quad 0 \leq t < \infty, \quad (28.b)$$

$$p_{xx} + p_{yy} + u_x^2 + 2v_x u_y + v_y^2 = G,$$
$$0 \leq x \leq L, \quad 0 \leq y \leq 1, \quad 0 \leq t < \infty. \quad (28.c)$$

We choose the forcing functions F_1, F_2, and G in such a way that the steady state solution is

$$u = \sin(2\pi n y) \cdot \{\sin(2\pi m(x-L)) + 2\} + 8 \cdot (y - y^2), \quad (29.a)$$

$$v = \frac{m}{n} \{\cos(2\pi n y) - 1\} \cdot \cos(2\pi m(x-L)), \quad (29.b)$$

$$p = \nu \cdot 2\pi m \cdot \sin(2\pi n y) \cdot \cos(2\pi m(x-L)). \quad (29.c)$$

The choice is done by inserting (29) in (28) and calculating F_1, F_2, and G analytically. We then implement the so-derived forcing functions in the program.

At $x = 0$ we apply the inflow boundary condition (1) with $r = 0$, where u_0 and v_0^r are defined by (29.a), (29.b) for $x = 0$. At $x = L$ we apply the outflow boundary condition (2) with $j = 2$, $q = 1$, where p_0 is defined by (29.c) for $x = L$. At $y = 0$ and at $y = 1$ we apply the solid wall condition $u = v = u_x + v_y = 0$. Hence, the boundary conditions are compatible with the steady state solution. As initial condition we use (29). The viscosity used in the tests is $\nu = 0.02$.

We run the program to steady state and compare the numerically calculated solution with (29). In Table I we show the results for different gridspacing in a low-frequency

TABLE I

Low Frequency Test, $m = 2$, $n = 2$, $L = \frac{7}{8}$

N_x, N_y	$\lvert\Delta u\rvert_\infty$	Order	$\lvert\Delta v\rvert_\infty$	Order	$\lvert\Delta p\rvert_\infty$	Order
8, 10	4.9 E−1		2.7E−1		1.1	
16, 20	4.8 E−2	3.4	3.0E−2	3.2	9.9E−2	3.5
24, 30	7.4 E−3	3.8	4.7E−3	3.7	1.5E−2	3.9
32, 40	1.8 E−3	4.0	1.2E−3	3.9	4.1E−3	4.0
48, 60	3.1 E−4	4.1	2.2E−4	4.0	7.1E−4	4.1
64, 80	1.17E−4	4.0	8.3E−5	3.9	2.1E−4	4.1

TABLE II

High Frequency Test, $m=3$, $n=4$, $L=\frac{11}{12}$

N_x, N_y	$\lvert\Delta u\rvert_\infty$	Order	$\lvert\Delta v\rvert_\infty$	Order	$\lvert\Delta p\rvert_\infty$	Order
24, 30	5.5 E−2		1.86E−2		8.3 E−2	
32, 40	1.39E−2	4.8	4.7 E−3	4.8	2.1 E−2	4.8
48, 60	1.76E−3	5.0	9.8 E−4	4.2	3.5 E−3	4.6
64, 80	6.0 E−4	4.6	4.8 E−4	3.7	1.57E−3	4.0

test with $m=2$, $n=2$, and $L=\frac{7}{8}$ in (29). In Table I we have defined the maximum error in u as $|\Delta u|_\infty = \max_{i,j} |u(i\cdot\Delta x, j\cdot\Delta y, \infty) - u_{i,j}(\infty)|$, where $u(i\cdot\Delta x, j\cdot\Delta y, \infty)$ is defined by the analytic steady state solution (29) and $u_{i,j}$ is the numerical steady state solution. The order of accuracy for u is defined as

$$\text{order} = \frac{\log(|\Delta u|_{\infty \text{ on the actual mesh}} / |\Delta u|_{\infty \text{ on the coarsest mesh}})}{\log(\Delta y_{\text{on the actual mesh}} / \Delta y_{\text{on the coarsest mesh}})}.$$

For instance, the order of accuracy in u on the (24, 30)-grid is calculated as

$$\text{order} = \frac{\log(0.0074/0.49)}{\log(30^{-1}/10^{-1})} = 3.8.$$

The accuracy for v and p are defined similarly.

In Table II we show the results for different gridspacing in a high-frequency test with $m=3$, $n=4$, and $L=\frac{11}{12}$ in (29). From Table I and II we see that the spatial convergence rate is approximately four.

6.2. Computational Results

In this section we present calculations that show the effect of different boundary conditions. We will see that the analytical results of the linear theory in Sections 2–5 hold true for the non-linear problem as well. That is, the boundary layers at the inflow are suppressed by as inflow condition prescribing (1) with r large, and at outflow by an outflow condition prescribing (2) with j and q large. The importance of choosing $j=q+1$ for large viscosity in order to obtain the solution divergence free is illustrated. Furthermore, the boundary conditions (1) and (2) give stable solutions of the non-linear problem.

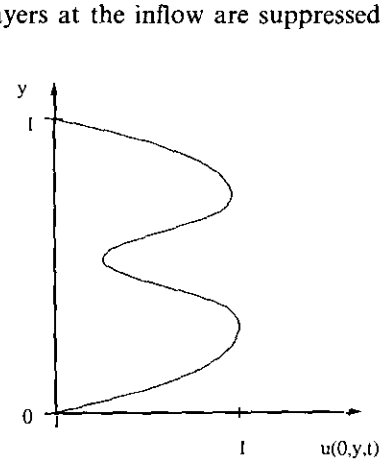

FIG. 2. The inflow velocity profile.

We will present numerical solutions of the time-dependent, incompressible Navier–Stokes equation (3) in a two-dimensional straight channel. A rectangular grid was used in all the calculations. We used the same inflow velocity profile in all the calculations and tested the different boundary conditions derived in Section 5. We also varied the viscosity ν. We did not vary the grid spacing Δx and Δy. The used inflow velocity profile, $u(0, y, t) = u_0(y)$, is shown in Fig. 2.

The variation in the y-direction was introduced for two purposes. One was to illustrate the existence of boundary layers at the inflow boundary. The other was to create a flow that varied in both the x- and y-directions at the outflow boundary. Thereby the effect of different boundary conditions, for inflow as well as for outflow, could be studied. We will especially investigate how efficiently different boundary conditions suppress the boundary layers. As initial condition we used $u(x, y, 0) = u_0(y)$, $v(x, y, 0) = 0$, and $p(x, y, 0) = 0$. In all the examples we run the program to steady state and show the so-derived solution.

Inflow

We now present how the inflow condition (1) affects the solution of the non-linear problem. We show surface plots of u, u_x, u_{xx}, v, v_x, and v_{xx}. We compare the results for $r=0$, $r=1$, and $r=2$. We let u_0 be the profile shown in Fig. 2 and $v_0^r = 0$. As the outflow condition we use $u_{xxx} = v_{xx} = p = 0$ at $x = L$. We will show the results for $\nu = 0.005$ and for $L = 1.25$.

Figure 3a shows surface plots of u, u_x, u_{xx}, v, v_x, and v_{xx} for the case when the inflow condition (1) with $v_0^r = 0$ and $r=0$ is used. We do not see any boundary layer in u. However, u_x vanishes at the boundary and attains a value that is $O(1)$ outside a boundary layer. This means that the boundary layer part and the interior part of u_x have the same magnitude. Finally, for u_{xx} we see a strong boundary layer (u_{xx} attains the value 14 at the boundary). The conclusion is that u_x and u_{xx} contain a boundary layer, whereas u does not.

We now consider v, v_x, and v_{xx} in Figure 3a. Here we see a boundary layer both in v, v_x, and v_{xx}. Note that each derivative makes the function approximately a factor 15 larger.

All this is in good agreement with the linear theory in Section 5.1. Indeed, from (14) we see that the strength of the inflow boundary layer in u and v in the linear case is

$$|\alpha_1/\alpha_u| = |\kappa_2/\omega|^{r+1} \tag{30.a}$$

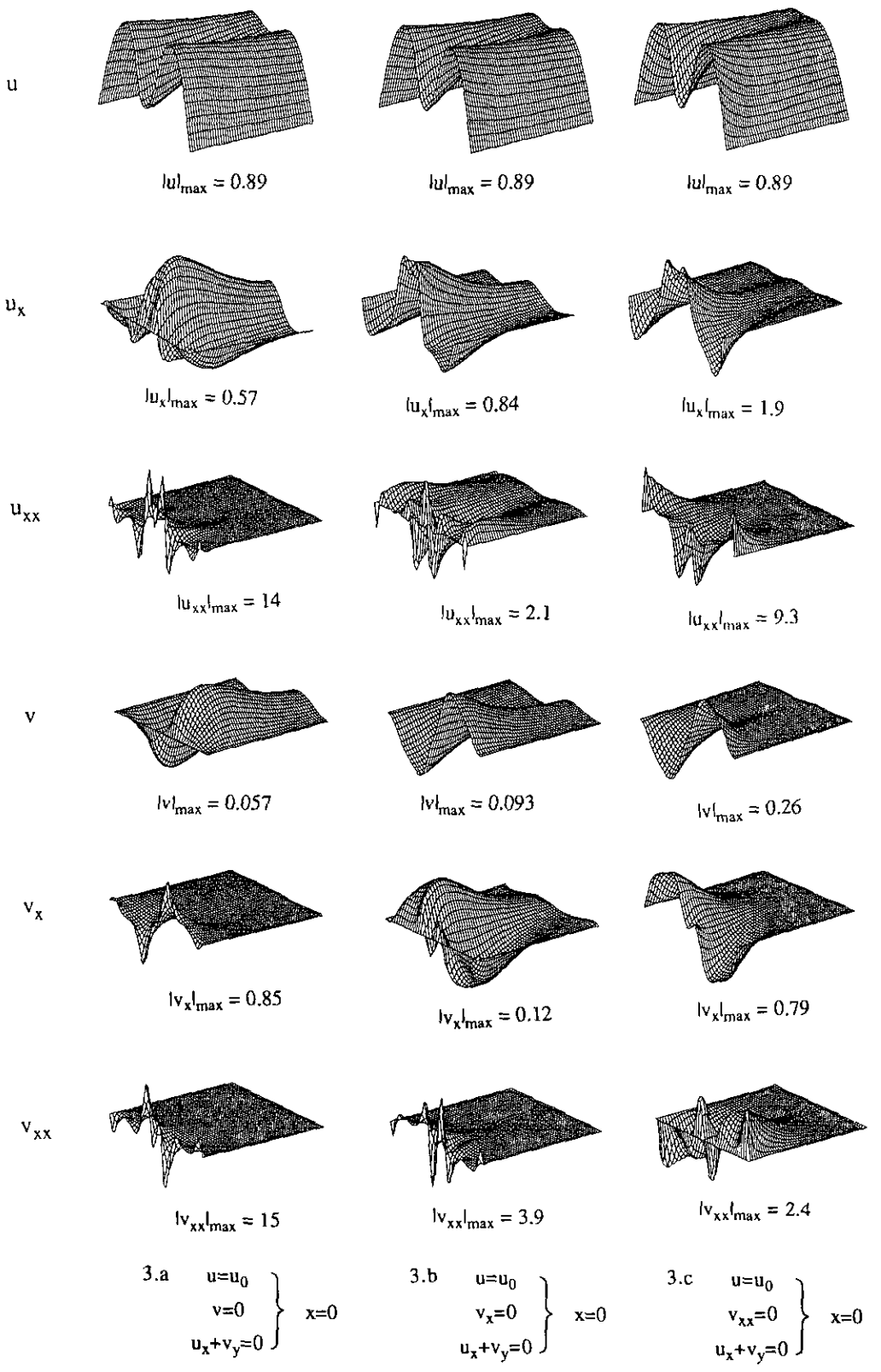

FIG. 3. Surface plots of u, u_x, u_{xx}, v, v_x, and v_{xx} for the steady state solution of the non-linear equation (3). The result for three different inflow boundary conditions at $x=0$ are compared. Under each plot the maximum absolute value is given. The inflow is to the left and the outflow is to the right. $L=1.25$. In (3.a) ($v=0$ at $x=0$) we see an inflow boundary layer in u_x, u_{xx}, v, v_x, and v_{xx}. In (3.b) ($v_x=0$ at $x=0$) we see an inflow boundary layer in u_{xx}, v_x, and v_{xx}. In (3.c) ($v_{xx}=0$ at $x=0$) we see an inflow boundary layer only in v_{xx}.

and

$$|\alpha_1/\alpha_v| = |\kappa_2/\omega|^r, \tag{30.b}$$

respectively. For the non-linear case we can make the rough estimate $|\omega| \approx \max_y |u_y(0, y, t)|/\max_y |u(0, y, t)| \approx 6$. According to Section 4.2 we have that in the inflow case $\alpha_1 \cdot e_1 \cdot e^{-|\omega|x}$ is the boundary layer part of the fundamental solution (6) and therefore the boundary layer thickness is $1/|\omega| \approx \frac{1}{6}$. This stands in agreement with the thickness seen in Fig. 3.a.

For U we in the non-linear case make the rough estimate $U \approx \int_0^1 u(0, y, t)\, dy \approx 0.5$. With $\nu = 0.005$ we obtain the rough estimate $\nu |\omega|/U \approx 0.005 \cdot 6/0.5 \approx 0.05 \ll 1$. Furthermore, the equations for steady state are the same as the Laplace transformed equations with $s = 0$. By (8.b), with $V = 0$, we therefore obtain $\kappa_2 \approx \nu\omega^2/U$. Letting $r = 0$ in (30) we now obtain that the strength of the boundary layer in u is

$$\left|\frac{\alpha_1}{\alpha_u}\right| = \left|\frac{\kappa_2}{\omega}\right| \approx \frac{\nu |\omega|}{U} \approx 0.05 \ll 1$$

and that the strength of the boundary layer in v is

$$\left|\frac{\alpha_1}{\alpha_v}\right| = \left|\frac{\kappa_2}{\omega}\right|^0 = 1.$$

Hence, according to the linear theory, no boundary layer should be seen in u, and the boundary layer part and the interior part of v should be equally strong. The u- and v-plots in Fig. 3a show that this is also the case for the non-linear problem.

From (6) we see that taking the x-derivative of u and v makes the boundary layer part $e^{-|\omega|x}$ of the solution a factor $|\omega|$ larger, whereas the interior part $e^{-\kappa_2 x}$ is multiplied by $\kappa_2 \approx \nu\omega^2/U$. This means that the boundary layers in u_x and v_x are a factor $|\omega|/\kappa_2 \approx U/\nu |\omega| \gg 1$ stronger than those in u and v. Hence, the strength of the boundary layer in u_x is

$$\frac{U}{\nu |\omega|}\left|\frac{\alpha_1}{\alpha_u}\right| \approx 1$$

and the strength of the boundary layer in v_x is

$$\frac{U}{\nu |\omega|}\left|\frac{\alpha_1}{\alpha_v}\right| \approx \frac{U}{\nu |\omega|} \gg 1.$$

That is, according to the linear theory, the inflow boundary layer should be seen both in u_x and v_x. For u_x the boundary layer part and the interior part should be equally strong. For v_x, the boundary layer part should be dominant. As seen in the u_x- and v_x-plots in Fig. 3a, this is also the case for the non-linear problem.

In the same way we from (6) see that taking another x-derivative of u and v makes the boundary layers another factor $|\omega|/\kappa_2 \approx U/\nu |\omega| \gg 1$ stronger. Hence, in the linear case, the strength of the boundary layer in u_{xx} is

$$\left(\frac{U}{\nu |\omega|}\right)^2 \cdot \left|\frac{\alpha_1}{\alpha_u}\right| \approx \frac{U}{\nu |\omega|} \gg 1$$

and the strength of the boundary layer in v_{xx} is

$$\left(\frac{U}{\nu |\omega|}\right)^2 \cdot \left|\frac{\alpha_1}{\alpha_v}\right| \approx \left(\frac{U}{\nu |\omega|}\right)^2 \gg 1.$$

This is in good agreement with the non-linear case presented in Fig. 3.a, where the inflow boundary layer is strong both in u_{xx} and v_{xx}.

In Fig. 3.b we show surface plots of u, u_x, u_{xx}, v, v_x, and v_{xx} for the case when the inflow condition (1) with $v_0^r = 0$ and $r = 1$ is used. Hence, at $x = 0$ we give $v_x = 0$ instead of $v = 0$ as the inflow condition. We see that we obtain an inflow boundary layer in u_{xx}, v_x, and v_{xx}, but not in u, u_x, or v. We also see that u, u_x, and u_{xx} have the same order of magnitude. Furthermore, v and v_x have the same order of magnitude, whereas v_{xx} is about a factor 30 larger than v_x. With the same arguments as when considering Fig. 3a we see that all this is in good agreement with the linear theory.

In Fig. 3.c we again show surface plots of u, u_x, u_{xx}, v, v_x, and v_{xx}, but the calculations are now made with the inflow condition (1) with $v_0^r = 0$ and $r = 2$ ($v_{xx} = 0$ at $x = 0$ instead of $v = 0$ at $x = 0$). We see an inflow boundary layer in v_{xx}, but not in u, u_x, u_{xx}, v, or v_x. Again, this is in good agreement with the linear theory.

The general conclusion from Fig. 3 is that the higher order of the x-derivative of v we set to zero at $x = 0$, the weaker the inflow boundary layer will be, exactly as predicted by the linear theory.

After the proof of Theorem 5.1 we point out that using the boundary condition $v_{xxx} = 0$ at $x = 0$, i.e., $r = 3$ in (1), is bad in case we have $\nu \ll 1$. This is because the solution might grow, even if u_0 does not, [2]. We have numerically solved the non-linear equation (3), together with this inflow condition as well. As predicted by linear theory, it turned out that the non-linear solution grew in time, so that no steady state solution was obtained. Hence, the only usable inflow boundary conditions are (1) with $r = 0$, 1, or 2.

Outflow

We now present how the outflow condition (2) affects the solution of the non-linear problem. We will compare the results for five different combinations of j and q, namely,

$$(j, q) = (1, 1), (1, 2), (2, 2), (2, 1), (3, 2).$$

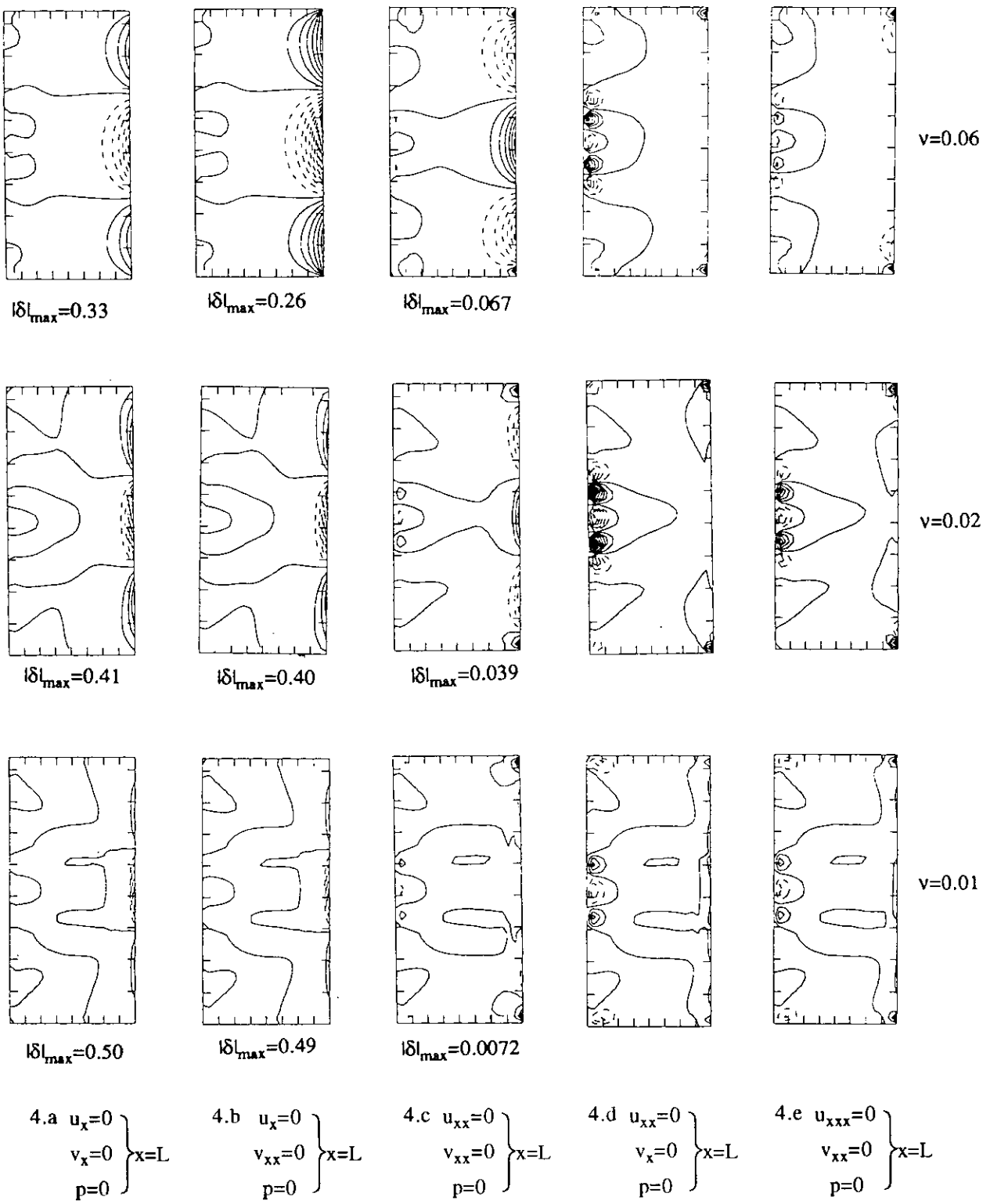

FIG. 4. The divergence $\delta = u_x + v_y$ in the solution of the non-linear equation (3) for different outflow boundary conditions and for different values of the viscosity. We obtain an outflow boundary layer in the divergence when $j \neq q+1$ (Figs. 4.a, b, c). The maximum absolute value of the divergence in this boundary layer is given under each plot in Figs. 4.a, b, c. Note that the outflow boundary layers become thinner the smaller the viscosity is. Furthermore, the layers are weaker if $u_{xx} = v_{xx} = 0$ is used (Fig. 4.c) than if $u_x = v_x = 0$ is used (Fig. 4.a). In case $j = q+1$ we do not obtain any outflow boundary layer in the divergence (Figs. 4.d, e). In these plots we see a small divergence at the inflow boundary. Due to automatic scaling in the plot program this small divergence is seen, even though it is much smaller than the divergence in Figs. 4.a, b, c. The inflow is to the left and the outflow is to the right. $L = 0.5$.

We let $p_0 = 0$ and as the inflow condition we use $u = u_0$, $v_{xx} = 0$, and $u_x + v_y = 0$ at $x = 0$. The calculations presented in Fig. 4 are made with the channel length $L = 0.5$, and the calculations presented in Fig. 5 are made with the channel length $L = 1.25$.

The linear theory in Section 5.2 shows that the solution of the linear problem contains outflow boundary layers in u and v. According to (18) and (8.b) (remember that $U < 0$ in the outflow case), these layers for $\nu \ll |U|/|\omega|$ are of the strength

$$\left|\frac{\alpha_u}{\alpha_1}\right| = \left|\frac{\omega}{\kappa_2}\right|^j < \left|\frac{\nu\omega}{U}\right|^j \ll 1$$

$$\left|\frac{\alpha_v}{\alpha_1}\right| = \left|\frac{\omega}{\kappa_2}\right|^q < \left|\frac{\nu\omega}{U}\right|^q \ll 1,$$

respectively. Hence, the higher the values of j and q that we choose in the linear case, the weaker the outflow boundary layers will be. The boundary layer thickness is $\nu/|U|$.

If $j = q + 1$ the solution of the linear continuous problem is divergence free. On the other hand, if $j \neq q + 1$, the solution will contain divergence that is confined to the outflow boundary layer.

To see how well the conclusions from the linear theory hold in the non-linear case, we choose to present plots of the divergence. Figure 4 shows the divergence in the non-linear case for different outflow boundary conditions and for different values of the viscosity. The viscosity is so large that the outflow boundary layers are resolved ($\nu = 0.06$, $\nu = 0.02$, and $\nu = 0.01$, corresponding to the cell Reynolds number $\mathrm{Re}_c = \Delta x/\nu = 0.42$, 1.25, and 2.5). We see that only the solutions plotted in Figs. 4.a, b, c, where $j \neq q + 1$, contain an outflow boundary layer in the divergence. The thickness of this layer is approximately proportional to ν. $|\delta|_{\max} = \max_{x,y} |\delta|$ is in Figs. 4a, b, c attained at the outflow boundary and can therefore be used as a measure of the strength of the boundary layer. Comparing the values of $|\delta|_{\max}$ in Fig. 4a and Fig. 4c yields that the boundary layers are weaker when $u_{xx} = v_{xx} = p = 0$ is used as the outflow condition than when $u_x = v_x = p = 0$ is used.

In Fig. 5 we show examples of what happens when the viscosity is so small that the outflow boundary layers are not resolved. In this case it is important to suppress the out-

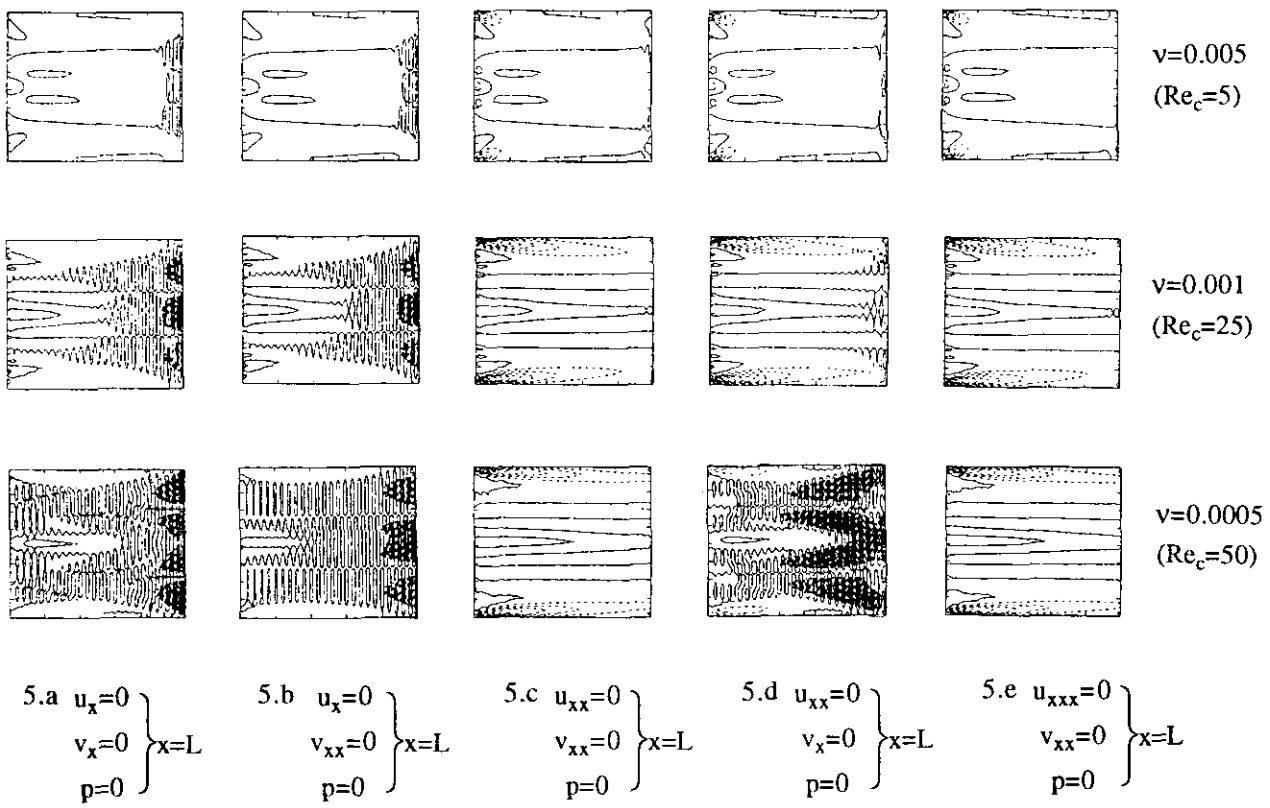

FIG. 5. The same calculations as in Fig. 4, but now for so small a viscosity that the outflow boundary layer is not resolved. This is so because the cell Reynolds number $\mathrm{Re}_c = \Delta x/\nu$ is large. In this case it is no longer important to have the condition $j = q + 1$ fulfilled. It is more important to choose j and q large so that the outflow boundary layers become weak. The only calculations with good results are those shown in Figs. 5.c, e, where both j and q are at least 2. In Figs. 5.a, b, d, where at least one of j and q equals 1, we see wiggles starting at the outflow boundary. The inflow is to the left and the outflow is to the right. $L = 1.25$.

flow boundary layers in u and v, as these layers otherwise will lead to wiggles. We see that the numerical solution (illustrated with the divergence) is well behaving at the outflow boundary in Figs. 5.c, e, where $j \geq 2$ and $q \geq 2$. On the other hand, in Figs. 5a, b, where $j = 1$, for $\nu = 0.0005$ and for $\nu = 0.001$ we obtain large wiggles, starting at the outflow boundary. For $\nu = 0.0005$ the wiggles are strong also in Fig. 5d, where $j = q + 1 = 2$. This shows that, when ν is so small that the outflow boundary layers are not resolved, due to the coarseness of the mesh used, $j = q + 1$ is not a sufficient condition to derive a well-behaving solution. Figure 5.c, where $j = q = 2$ is used with good result, shows that the condition $j = q + 1$ is not even necessary. Instead we must choose j and q so large ($j \geq 2$ and $q \geq 2$) that the outflow boundary layers are properly suppressed.

All the conclusions above are in good agreement with the linear theory in Section 5.2.

7. SUMMARY

As inflow boundary conditions we suggest

$$\begin{pmatrix} u \\ \dfrac{\partial^r v}{\partial x^r} \\ u_x + v_y \end{pmatrix} (0, y, t) = \begin{pmatrix} u_0 \\ v_0^r \\ 0 \end{pmatrix} (y, t), \qquad r = 0 \text{ or } 1 \text{ or } 2.$$

If the assumptions in Section 4.2 are fulfilled; i.e., if the viscosity ν is small, there might be boundary layers in the solution. The larger r we use (i.e., the higher the order of the x-derivative of v we prescribe), the weaker will this boundary layer be, provided that we let $v_0^r = 0$. However, for $r \geq 3$ the solutions can grow in time even if u_0 and v_0^r do not. We therefore recommend to use $v_{xx} = 0$ as the inflow boundary condition.

If the boundary condition $u_x + v_y = 0$ at $x = 0$ is not properly fulfilled, that is if we instead give $u_x + v_y = d_0 \neq 0$, this boundary condition will act as a source of divergence. This divergence will not be confined to the boundary. Therefore, it is very important that the condition $u_x + v_y = 0$ at $x = 0$ is fulfilled.

Finally, note that complementing the no-slip condition $u = v = 0$ at $x = 0$ with the condition $u_x + v_y = 0$ at $x = 0$ yields a special case of the above condition, namely $r = 0$, together with $u_0 \equiv v_0^0 \equiv 0$. Furthermore, complementing the slip condition $u = v_x = 0$ at $x = 0$ with the condition $u_x + v_y = 0$ at $x = 0$ yields another special case of the above condition, namely $r = 1$, together with $u_0 \equiv v_0^1 \equiv 0$.

As outflow boundary conditions we suggest

$$\begin{pmatrix} \dfrac{\partial^j u}{\partial x^j} \\ \dfrac{\partial^q v}{\partial x^q} \\ p \end{pmatrix} (0, y, t) = \begin{pmatrix} 0 \\ 0 \\ p_0 \end{pmatrix} (y, t).$$

If $\nu \ll 1$ the solution will contain a boundary layer part that we want to suppress. This is done by choosing $j \geq 1$ and $q \geq 1$. The larger j and q we choose, the more suppressed will the boundary layer be.

In order to make the solution divergence free we must let $j = q + 1$. However, if $\nu \ll 1$ it is not very important to fulfill this requirement, as the divergence will in this case be confined to the outflow boundary layer, which we suppress by choosing j and q large. We recommend to use $j = 3$ and $q = 2$. In case the viscosity is small, we can also use $j = 2$ and $q = 2$.

ACKNOWLEDGMENTS

Professor Bertil Gustafsson and Professor Heinz-Otto Kreiss are gratefully acknowledged for many fruitfull discussions on the present problem. This project was financed by The Swedish Institute of Applied Mathematics (ITM), STU Contract 88-01599P and Navy Contract N-00014-83-K-0422. All these contributions are very much appreciated.

REFERENCES

1. L. V. Ahlfors, *Complex Analysis*, 3rd ed. (McGraw–Hill, New York, 1979).
2. C. Johansson, *Initial-Boundary Value Problems for Incompressible Fluid Flow* Doctoral thesis in Numerical Analysis, March 1991. Uppsala University, Department of Scientific Computing, Box 120, S-751 04 Uppsala, Sweden (unpublished).
3. C. Johansson, Well-posedness in the generalized sense for the incompressible Navier–Stokes equation, *J. Sci. Comput.* **6** (2), 101 (1991).
4. C. Johansson, Well-posedness in the generalized sense for boundary layer suppressing boundary conditions, *J. Sci. Comput.* **6** (4), 391 (1991).
5. H.-O. Kreiss and J. Lorenz, *Initial-Boundary Value Problems and the Navier–Stokes Equations* (Academic Press, New York/London, 1989).
6. M. J. Naughton, *On Numerical Boundary Conditions for the Navier–Stokes Equations*, Ph.D. thesis, California Institute of Technology, Pasadena, California, 1986 (unpublished).
7. R. A. Sweet, A cyclic reduction algorithm for solving block tridiagonal systems of arbitrary dimension, *SIAM J. Numer. Anal.* **14**, 706 (1977).